Continental Shelf Research 277 (2024) 105248

Contents lists available at ScienceDirect

Continental Shelf Research

journal homepage: www elsevier com/locate/csr

Research papers

Drivers of neritic water intrusions at the subtropical front along a narrow shelf

Erik E. Johnson [a,*], Charine Collins [b], Sutara H. Suanda [c], Stephen R. Wing [a], Kim I. Currie [b], Jesse Vance [d], Robert O. Smith [a]

[a] Department of Marine Science, University of Otago, 310 Castle Street, Dunedin, 9016, Otago, New Zealand
[b] NIWA, 301 Evans Bay Parade, Wellington, 6021, Wellington, New Zealand
[c] Department of Physics and Physical Oceanography, University of North Carolina Wilmington, 601 South College Road, Wilmington, 28403-5606, NC, USA
[d] Climate Global Dynamics Laboratory, NCAR, 1850 Table Mesa Dr, Boulder, 80305, CO, USA

ARTICLE INFO

Keywords:
River plume
Subtropical front
Freshwater influence
Numerical modelling
Cross-isobath flow

ABSTRACT

The near-ubiquitous presence of freshwater over the inner to mid-continental shelf off of the Otago Peninsula in southeast Aotearoa/New Zealand has been previously identified in long-term cross-shelf transects. Occasional influxes of this silicate-rich neritic water past the shelf break and beyond the Subtropical Front have been observed, potentially supporting elevated chlorophyll-a concentrations in SubAntarctic waters. Nearshore salinity variability has been connected to flow rates of the Clutha River, Aotearoa's largest river by discharge, however, other physical mechanisms influencing the structure of freshwater along this coast have not been explicitly explored. A numerical model of Aotearoa's southeast continental shelf forced with realistic discharge from the Clutha River is used to assess the drivers of river plume variability and identify conditions associated with the transport of neritic water beyond the shelf break. Event scale, lagged correlation, EOF, and composite analysis of a model passive dye tracer revealed three generalised plume structures that are dependent on river discharge, along-front wind stress, and shelf current velocities. Downfront wind stress suppresses bulge formation at the river mouth and constrains the river plume against the coast, whereas upfront wind stress causes the river plume to move offshore over the shelf and spread across the upper water column. Rarely, upfront wind stress generates a nearshore current reversal over the shelf, causing the plume to deflect straight off-shelf and across the shelf edge before meeting the frontal current and advecting to the northeast. Future observational work is required to validate the mechanisms described and address the biological implications of these findings.

1. Introduction

1.1. Freshwater interactions at the Southland Front

Terrestrial river outflows represent dominant sources of sediments, nutrients, pollution, and buoyancy for many coastal systems (Schiller et al., 2011; Sharples et al., 2017; Masotti et al., 2018), driving variability in nearshore water quality, stratification, and primary productivity. River plumes tend to form coastally constrained buoyancy currents, limiting direct interactions between river discharge and off-shelf waters (Yankovsky and Chapman, 1997; Chant et al., 2008; Horner-Devine, 2009). However, both observational and modelling studies have identified physical processes (*eg.* wind stress, discharge, coastal currents) that detach river plumes from the coast (García Berdeal, 2002; Choi and Wilkin, 2007; Hickey et al., 2009; Warrick and Stevens, 2011), in some cases advecting low salinity water over 50 km offshore. At narrow continental shelves, these detachment events may allow river plumes to move beyond the shelf break and directly interact with open ocean waters, modifying stratification, supplying limiting nutrients, and facilitating phytoplankton blooms.

The shelf break region surrounding Ōtākou/the Otago Peninsula is globally unique on account of the proximity between the Subtropical Front, marking the northern limit of the Southern Ocean, and significant terrestrial freshwater input (Jillett, 1969; Jones et al., 2013; Chiswell et al., 2015). A combination of factors contributes to this phenomenon: a relatively narrow shelf break (20 km wide off of the Otago Peninsula) (Chiswell, 1996; Hawke, 1989), proximity to the Mata-Au/Clutha River (Aotearoa/New Zealand's (ANZ) largest river by discharge) (Murray, 1975; Jillett, 1969; Hawke, 1992), and

* Corresponding author.
E-mail address: erik-johnson@live.ca (E.E. Johnson).

https://doi.org/10.1016/j.csr.2024.105248
Received 2 November 2023; Received in revised form 28 April 2024; Accepted 5 May 2024
Available online 8 May 2024

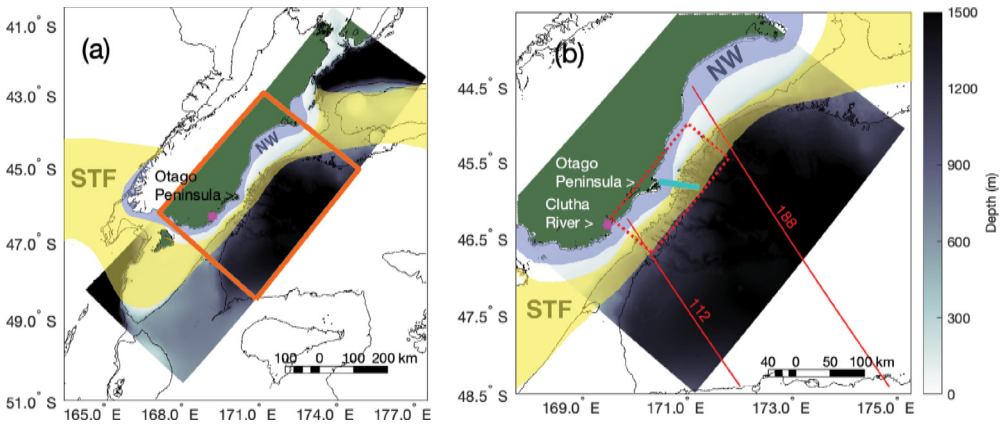

Fig. 1. (a), Full spatial extent of the model domain. (b), Subset of the model domain that is the focus of this study. Yellow shading indicates area coinciding with the Subtropical Front (STF), purple shading indicates neritic water (NW). Red dashed box shows the area over which wind stress and shelf velocities are averaged, cyan line shows the position and extent of the *in situ* Munida Transect, solid red lines indicate altimetry tracks used in model validation. The mouth of the Mata-Au/Clutha River is marked by a purple dot.

a topographically-steered section of the Subtropical Front (locally referred to as the Southland Front) (Chiswell, 1996; Hopkins et al., 2010; Stevens et al., 2019). As a result, three water masses characterise this narrow shelf: nearshore neritic water (NW), freshwater-modified subtropical water (STW) over the mid to outer shelf, and off-shelf SubAntarctic water (SAW) (Jillett, 1969; Murdoch et al., 1990; Jones et al., 2013). Generally, NW is the least saline and warmer/cooler than STW water in the summer/winter (Jillett, 1969; Hawke, 1992). STW is both more saline and warmer than SAW (Jillett, 1969; Hopkins et al., 2010), forming the strong thermohaline gradient that marks the Southland Front. This shelf break front is associated with a strong northeast flowing boundary current, known as the Southland Current (Heath, 1972; Chiswell, 1996; Fernandez et al., 2018). SAW is considered a high-nutrient low-chlorophyll water mass, rich in nitrate and phosphate but poor in micronutrients such as iron, resulting in low productivity (Boyd et al., 2004; Baltar et al., 2015). Over the shelf, STW is often depleted in macronutrients, but rich in micronutrients sourced from the shelf-bed and terrestrial runoff (Croot and Hunter, 1998; Jones et al., 2013; Durante et al., 2021). Despite the large agricultural area in the Clutha Catchment, NW is generally nitrate and phosphate-poor, instead representing the dominant supply of silicate to the shelf (Croot and Hunter, 1998).

Instances where NW extends across the shelf break front into SAW have been documented in prior studies of this region (Murdoch et al., 1990; Haywood, 2004; Jones et al., 2013), and it has been suggested that this interaction may supply silicate and iron to SAW, supporting the growth of silicic diatoms (Boyd et al., 2004; Haywood, 2004; Jones et al., 2013; Baltar et al., 2015), and driving blooms in usually low-chlorophyll offshore waters. To date, the understanding of physical processes that drive cross-front intrusions of NW is limited for this region, with most studies of this coast relying on temporally coarse sampling (monthly or greater). Recent work (Johnson et al., 2023) has highlighted significant subseasonal variability in shelf hydrography in response to along-front wind forcing. Still, the processes affecting the intensity and offshore extent of the Clutha River plume have not yet been explicitly investigated on these time scales. This region is historically and culturally significant to the Māori of southern ANZ, in addition to supporting at-risk endemic species (Augé et al., 2012), and commercially significant fisheries (Waugh et al., 2005; Leathwick et al., 2006). Understanding the mechanisms that control the cross-shelf exchange of nutrients, and the scope of interaction between freshwater, the Subtropical Front, and offshore SAW is critical to the understanding of this system as a whole.

1.2. Potential mechanisms driving NW-front interactions

Though the nearshore presence of NW has been thoroughly documented as a quasi-permanent feature, it is marked by significant variability in salinity and offshore extent (Hawke, 1992; Murdoch et al., 1990; Jones et al., 2013). The occurrence of local minima in salinity 15 km off of the Otago Peninsula has been connected to changes in Clutha River discharge (Q) 4–12 days prior; coarsely establishing the timescales of downstream plume advection and residence time between the river mouth and Otago Peninsula (distance of roughly 100 km) (Hawke, 1992). Despite the operation of several hydroelectric dams along tributaries of the Clutha, limited storage capacity means that the resulting flow rates are similar to natural flow patterns (Murray, 1975). This corresponds to a seasonal cycle that peaks during December (mean 682 m^3s^{-1}), as a result of high-alpine snowmelt in the catchment, as well as a smaller peak in May (mean 590 m^3s^{-1}). The mean Q is approximately 500 m^3s^{-1} with limited seasonal variability in monthly means (±180 m^3s^{-1}) that is smaller than the standard deviation in most months (Murray, 1975). Flood events can exceed 3000 m^3s^{-1}, strongly influencing shelf hydrography and potentially driving the influx of riverine waters at the shelf break front (Murray, 1975; Jones et al., 2013).

Beyond increasing the volume of NW over the shelf, it is not well-known how the Clutha River plume affects shelf circulation. Large river plumes can form "bulges" at the river mouth, associated with an anticyclonic circulation that increases the residence time of freshwater over the shelf (Chao and Boicourt, 1986; Horner-Devine, 2009; Hickey et al., 2010; Moffat and Lentz, 2012; Saldías et al., 2012). The offshore extent reached by this bulge can be approximated from:

$$y_s = R_{di}\frac{2\ 3+F_i^2)}{2+F_i^2)^{1/2}} \quad (1)$$

Where $R_{di} = g' \times h_0)^{1/2}/f$ is the baroclinic Rossby radius (in m) of the river inflow, and $F_i = v_i/\ g' \times h_0)^{1/2}$ is the inflow Froude number (Yankovsky and Chapman, 1997). Assuming that the Clutha River plume is completely fresh, and has a discharge of 1000 m^3s^{-1} (consistent with high-flow events; Murray, 1975), an inflow depth (h_0) of 2 m, and a river mouth width of 400 m (Mitchell et al., 2012), the estimated outflow velocity (v_i) is 1.25 ms^{-1}, and thus the offshore extent of a surface advected plume is 37 km. This radius would be within 5 km of the shelf break, suggesting that high discharge events have the potential to form a nearfield river plume adjacent to the Subtropical Front.

Owing to their buoyancy, river plumes in other systems have been shown to respond strongly to surface wind stress (Fong and Geyer, 2001; Choi and Wilkin, 2007; Hickey et al., 2009; Warrick and Stevens, 2011; Moffat and Lentz, 2012; Kakoulaki et al., 2014; Fernández-Nóvoa et al., 2017). In numerical models of the inner Mid-Atlantic Bight, upfront (generating offshore Ekman transport) wind stress caused a detachment of the coastally-trapped Hudson River plume (mean flow

rate of 460 m^3s^{-1}, comparable to that of the Clutha River), dispersing the low-salinity anomaly and moving the plume offshore, increasing nearshore salinity downstream and decreasing salinity over the mid-shelf (Choi and Wilkin, 2007). When winds were downfront (generating onshore Ekman transport), the plume was strongly constrained to the coast, driving low nearshore salinity downstream (Choi and Wilkin, 2007). Numerical modelling and *in situ* observations of the Columbia River plume in the Pacific Northwest, which is much larger than the Clutha and Hudson Rivers (4000–12000 m^3s^{-1}), found that coastal neritic water experienced more rapid surface Ekman transport as a result of the shallower mixed layer (Hickey et al., 2010). Due to the relatively narrow continental shelf along the Otago coast (Fig. 1), plume detachment and intensified Ekman transport following upfront winds are potentially able to transport NW to the Subtropical Front. The winds in this region oscillate frequently on the along-front axis (Kidson, 2000), which has been previously suggested to drive significant cross-shelf Ekman transport and frontal adjustment at the shelf break (Johnson et al., 2023).

Development of the Clutha River plume is likely further affected by the local boundary current, the Southland Current, due to the persistent and intense downfront flow over the shelf and shelf break that it generates (Hawke, 1989; Chiswell, 1996; Hopkins et al., 2010). The Southland Current has been described as variable in strength, but nearly unidirectional, flowing northeast with the exception of infrequent, short-lived, reversals over the shelf (Croot and Hunter, 1998; Chiswell, 1996). This variability in current strength potentially affects plume development, as the Clutha River plume theoretically follows a surface-advected regime in lieu of alongshelf forcing (Yankovsky and Chapman, 1997), resulting from the shallow inflow depth (approximately 2 m), rapid mean discharge velocity, and large density anomaly (assuming discharge is near 0 PSU). Downfront currents have been shown to inhibit bulge formation near river mouths and constrain the plume to the coast (Horner-Devine, 2009; Fernández-Nóvoa et al., 2017), and as such, variability in Southland Current velocity over the shelf and slope will likely impact the development of plume in both the near and far-field extent.

1.3. Study objectives

To date, the absence of 3-dimensional hydrographic data on fine spatiotemporal scales, has prohibited an investigation of mechanisms relevant to river plume structure and extent over the Otago Shelf. Previous work off of the Otago Peninsula has identified periods where the salinity minima associated with freshwater discharge exist variably as a relatively thin (10 m) surface lens over the mid-shelf, or a nearshore feature extending to the seabed (Murray, 1975; Jillett, 1969; Hawke, 1995; Jones et al., 2013). As these studies relied on observations collected along a single transect, often at monthly temporal resolution, the upstream structure of the Clutha River plume is unclear, as are the processes contributing to generating downstream variability. This study employs output from a realistic hydrodynamic numerical model of the Otago shelf, validated against long-term *in situ* observational data, to evaluate the behaviour of the Clutha River plume under historic discharge and wind stress. The 3-dimensional output of this model allows investigation of the downstream evolution of the Clutha River plume over spatial (hundreds of kilometers) and temporal scales (sub-daily) that are unattainable observationally.

The motivating questions behind this work are:

> How does the along and cross-shore structure of the freshwater plume vary? What is the influence of freshwater input and local winds on this variability?
> How frequently does nearshore neritic water interact with the shelf break front? What conditions drive these interactions?

Section 2.1 outlines the Regional Ocean Modelling System (ROMS) simulation of ANZ's Southeast shelf, which is first compared to historic observational data in Section 3.1 to verify the reasonable replication of observed patterns in regional hydrography. Subsequently, Section 3.2 investigates a time series of shelf and slope dye concentrations along the study region, then examines in detail three individual case studies where the Clutha River plume moved beyond the shelf break. Section 3.3 then uses empirical orthogonal functions (EOF) to generalise conditions that are associated with spatial patterns of the Clutha River plume. From this understanding, Section 3.4 presents lagged correlations between dye concentrations and potential driving mechanisms in order to identify relevant response times. Composite analysis is then presented in Section 3.5 to investigate dye concentration and circulation anomalies associated with various discharge and along-front wind stress (τ_a) scenarios. Section 4 then discusses the implications of these results concerning shelf hydrography and productivity for southeast ANZ, and narrow shelves in general.

2. Data methods

2.1. Model configuration

The hydrodynamic model used for this study is the Regional Ocean Modelling System (ROMS), a free-surface ocean model that solves the incompressible, hydrostatic, primitive equations based on the Boussinesq approximation and the hydrostatic vertical momentum balance (Shchepetkin and McWilliams, 2005). It is a split-explicit ocean model discretised in terrain-following curvilinear coordinates. A detailed description of the ROMS computational kernel is provided in Shchepetkin and McWilliams (1998) and Shchepetkin (2003).

The model domain was designed to encompass the entire east coast of Te Waipounamu/the South Island of ANZ from Snares Plateau in the south to Cook Strait in the north at a horizontal resolution of 2.5 km (Fig. 1a). In the vertical, it has 30 terrain-following vertical levels stretched towards the surface and seafloor, resulting in a vertical resolution of 1-10 m on the continental shelf and 5–250 m offshore. The model bathymetry was constructed from a number of different sources. The General Bathymetric Chart of the Oceans (GEBCO) one-minute resolution dataset was used for depths greater than 500 m. This dataset was combined with 250 m resolution bathymetric data from the National Institute of Water and Atmospheric Research (NIWA), land elevation data at 200 m resolution and high-resolution coastline position data from Land Information New Zealand.

The model was initialised on 1 January 2008 with initial and boundary conditions for the hydrodynamic variables, and ran for ten years (ending 24 October 2018). Model output was saved at 6-hour intervals. The lateral boundaries of the model domain were forced by a combination of tides (depth-averaged velocity and sea surface height) and subtidal oceanic conditions (temperature, salinity, depth-varying velocity). The subtidal lateral boundary conditions were obtained from a global ocean analysis and prediction system based on the Hybrid Coordinate Ocean Model (HYCOM) (Chassignet and Verron, 2006). The HYCOM product used here provides daily snapshots of the 3-dimensional state of the global ocean on a 1/12 grid. The tides imposed at the boundaries of the model domain were specified in terms of the amplitude and phase of 13 tidal constituents derived from the NIWA EEZ tidal model (Walters et al., 2001). The vertical eddy viscosity and diffusivity are computed using turbulence closure schemes incorporated into ROMS. For this simulation, the Large-McWilliams-Doney K-profile parameterization (KPP) scheme (Large and Gent, 1999) was implemented with background diffusivity (and background viscosity) set to a constant of $10^{-4}m^2s^{-1}$.

The model was forced at the surface with heat, momentum and freshwater fluxes. Surface heat and freshwater fluxes were derived from 6-hourly NCEP/NCAR reanalysis data (Kalnay et al., 1996). The

NCEP/NCAR reanalysis product provides global analyses of atmospheric fields at a 2.5 resolution. The surface wind stress was derived from 3-hourly winds obtained from the 12 km New Zealand Limited Area Model (NZLAM) (Lane et al., 2009).

All the rivers (149 total) draining into the ocean along the east coast of the South Island were represented in the model as point sources of freshwater. The rivers draining into the model domain were identified from the New Zealand River Environment Classification (Biggs et al., 1990; Snelder et al., 2010) and a constant annual-mean value of riverine freshwater input was used for all rivers except the Clutha River. Daily discharge for the Clutha River was obtained from NIWA's Hydro Web Portal from 2008–2017. ROMS's passive tracer computational capabilities were used to track the freshwater discharge from the Clutha River by tagging it with a dye tracer (conservative passive tracer). The dye has a unitless concentration with values between 0 and 1, and represents the concentration of the river freshwater, *i.e.* if the dye has a value of 1 it means the water parcel is purely river water; if it has a value of 0 it means the water parcel contains no freshwater from the Clutha River.

2.2. Observational data

The model was validated against surface *in situ* data from the Munida Transect (Currie et al., 2011), a multi-decade bi-monthly oceanographic transect off of the Otago Peninsula (cyan line, Fig. 1b). This data set provides 60 underway sea surface temperature (SST) and salinity traces coinciding with the model run, measured via a thermosalinograph from Sea-Bird Electronics (using a SBE21 until 2010, then SBE45 for salinity and SBE38 for SST), and averaged to 500 m cross-shelf increments.

Six-hourly wind fields were downloaded from the European Centre for Medium-Range Weather Forecasts' fifth generation re-analysis (ERA5) product (Hersbach et al., 2020) and averaged over the shelf region (dashed red box, Fig. 1b). ERA5 uses assimilated data from satellite and *in situ* observations, to produce a global atmospheric hindcast at 31-km resolution (Hersbach et al., 2020). This publicly available data set was used instead of the NZLAM winds that forced the model, as NZLAM is not publically available. Both ERA5 and NZLAM models are assimilated with *in situ* and ASCAT wind observations (Lane et al., 2009; Hersbach et al., 2020), so the wind stress over the shelf derived from ERA5 is presumably comparable.

L2P X-Track sea level altimetry (SLA) data was acquired from Archiving, Validation and Interpretation of Satellite Oceanographic data (AVISO+) along Jason-Orbit tracks 112 and 188, with 1 Hz resolution (approximately every 6–7 km) (Birol et al., 2017). This data set utilises SLA measurements from the Topex, Jason-1, Jason-2, and Jason-3 satellites, processed with the X-Track algorithm to improve data quality in coastal regions (Birol et al., 2017). Each track is repeated approximately once every 10 days, and the time series spans from 1993-present, covering the whole model run.

True colour Sentinel II L2 A imagery was acquired from the Sentinel Hub EO Browser for the study region. Images with low cloud cover (20) and clear optical signal of the Clutha River plume were selected. Preceding Q and τ_a were calculated for each image meeting these criteria.

2.3. Analysis

For comparing *in situ* observations to model output, model temperature and salinity fields at each depth level were first linearly interpolated to points along the Munida Transect at 2.5 km intervals (cyan line, Fig. 1b). Model data were then resampled with respect to time to generate a data set temporally consistent with the observations. The underway *in situ* observations were averaged to 2.5 km intervals to correspond to the resolution of the model.

X-Track SLA was first smoothed along each track with an optimal difference operator (Powell and Leben, 2004; Liu et al., 2012) before adding the mean dynamic topography and calculating geostrophic velocities. ROMS sea level heights were then interpolated to altimetry track locations and temporally resampled to correspond to X-Track data. Model geostrophic velocities were then calculated from the resampled ROMS dataset.

Model performance was evaluated using three metrics (outlined in Montaño et al. (2023)); mean model offset, root mean squared error (RMSE) and the Willmott Skill score (Willmott, 1981). These metrics were calculated at the aforementioned cross-shelf increments (2.5 km intervals for SST and salinity, 7 km intervals for altimetry), to examine performance at different portions of the shelf/slope.

To discern model velocities over the Ekman layer, a time series of mean velocity in the upper 45 m was calculated (approximately corresponding to the Ekman layer depth at 45 degrees latitude, assuming eddy-viscosity of 0.1 m^2/s). For each time step and grid point, model u and v velocity fields were interpolated to 1-meter increments and averaged over the upper 45 m. For grid cells less than 45 m deep, the velocities were averaged over the whole water column.

Wind vectors computed from ERA5 were rotated 40 degrees from north, corresponding to the average angle of the shelf break for this region. The along-front component of the wind stress was then computed at each grid cell, and data over land was omitted. From this, the median value within a box centred over the region of interest (red box, Fig. 1b) was computed. Anomaly time series were calculated for τ_a and Q by removing the monthly median which had been smoothed with a 3-month moving window.

A passive dye tracer was used instead of salinity to track the evolution of the Clutha River plume along the shelf. Due to low-salinity SAW off-shelf, instances where the plume passes the front are not always discernible by salinity fields alone. Furthermore, dye analysis eases calculating the percent Clutha River water by composition at any point along the shelf. Due to the rapid mixing of dye downstream from the Clutha, dye fields were often multiplied by 1000 and $\log_{10}$ scaled to ease visualisation. Median dye concentration over the shelf (inshore of the 500 m isobath) and slope (50 km offshore of the 500 m isobath) were binned at 0.25 latitudinal increments to generate a shelf/slope dye time series along the shelf break region. These time series were used to identify periods of elevated off-shelf dye concentrations for event analysis.

A time series of depth-integrated dye export was calculated across the 500 m isobath by interpolating dye concentrations, u, and v velocities to points spaced every 1 km along the 500 m isobath. Dye concentrations were multiplied by the time-varying thickness of each ROMS layer, and u/v components, providing the u and v areal export at each point. From this, the component normal to the angle of the 500 m isobath (angle smoothed with a 20 km filter) was computed.

Empirical orthogonal functions (EOFs) were computed using the EOF function provided in the Climate Data Toolbox for MATLAB (Greene et al., 2019) on log-scaled surface dye concentrations to identify the dominant spatial patterns of Clutha River plume variability. Tracer concentrations were log-scaled due to the near-logarithmic dilution of dye downstream of the Clutha River mouth. Without log-scaling, EOFs were dominated by the near-field river plume, offering little insight into patterns of plume extent downstream. To avoid large negative values skewing the EOF modes, log-scaled dye values below 0 (1 ppt), were set to zero. An EOF analysis generates two parts, a fixed spatial structure (EOF) and its time-dependent amplitude (principal component time series). The calculated EOF mode spatial structures have units of log-transformed dye concentration, and the principal components (or PC time series) are unitless. From these, the PC time series of relevant EOF modes were compared to binned Q and τ_a anomalies. Relevant modes were determined according to the North Test (Loughran et al., 2017), where only modes with non-overlapping uncertainty estimates are considered.

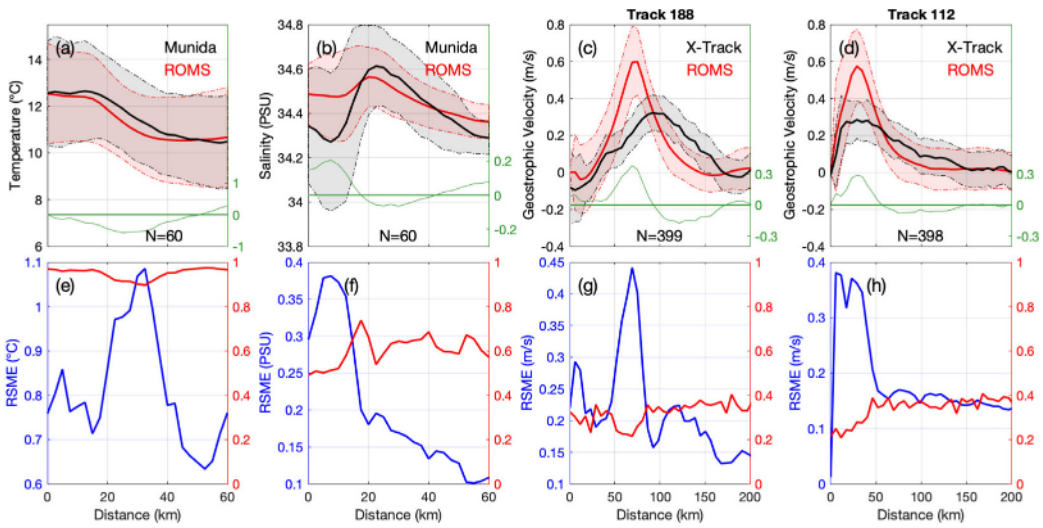

Fig. 2. Model skill evaluation for sea surface temperature (a,e), salinity (b,f) along the Munida Transect and geostrophic velocity along track 188 (c,g) and track 112 (d,h). Top panels show mean (solid lines), standard deviation (shaded area) on the left axis, and mean model offset (green line) on the right axis. Bottom panels show RMSE (blue, left axis), and Willmott skill score (red, right axis).

Lagged correlations were computed at each model grid cell between surface dye anomaly and Q/τ_a anomalies. For computational efficiency, correlations were computed at a maximum lag of 30 days. R-values indicating significance at a 99 confidence interval were calculated for each grid point using the modified Chelton method (Pyper and Peterman, 1998). R-values below this threshold were masked.

3. Results

3.1. Evaluation of model skill

Agreement between resampled ROMS surface temperature and *in situ* observations (N = 60) was strong, with variability in shelf and offshore temperatures well-represented (Fig. 2a). Generally, the model has a negative temperature bias over the thermal front (−0.5 C mean offset, Fig. 2a), where the Willmott skill slightly declines and RMSE increases (Fig. 2b). Offshore of the front (> 45 km) the RMSE is lowest, and Willmott skill is near 1, indicating a significant model-observation agreement.

The model produced a nearshore salinity depression associated with NW, but nearshore values were significantly higher than observations (Fig. 2b). The mean offset of nearshore salinity exceeded 0.2 PSU within 10 km of the coast, improving beyond the nearshore band of neritic water (Fig. 2b,f). Within 20 km of the coast, salinity variability was significantly underestimated. Both the RMSE and Willmott skill improved further offshore beyond the salinity maximum where salinity is less variable.

Peak mean ROMS along-track geostrophic velocities were significantly higher than X-Track observations for both tracks 188 and 112 (by a factor of 1.8 for track 188, and a factor of 2.1 for track 112, Fig. 2c,d). The position of the center of the shelf break current for track 188 is 25 km inshore in the model relative to observations (N = 399), resulting in a large RMSE 60 km along track (Fig. 2g). The ROMS placement for the Southland Current is better along track 112 (N = 398), although the mismatch in current strength also generates large RMSE over the shelf/slope (0–50 km, Fig. 2h). The Willmott skill is low (0.4) for both altimeter tracks, suggesting relative disagreement between the model and X-Track geostrophic current variability.

Seasonal patterns in shelf and offshore temperatures are well-represented (Fig. 3a,b). Offshore movement of temperature gradients during cooler months is accurately replicated, with the nearshore edge of the thermal front moving from 20 km along the transect to 35 km (Fig. 3a). Generally, the model has a negative temperature bias (−0.25 C on average), most pronounced over the shelf and front in summer months (mean −1 C at 25 km along the transect, Fig. 3c). The model produced a nearshore salinity depression associated with NW, but nearshore values were frequently higher than observations (Fig. 3d-f). Positive nearshore salinity biases were most prominent in Autumn and Winter, at times exceeding +0.25 PSU within 10 km of the coast (Fig. 3f). The salinity maximum of STW, and the decrease across the front to relatively fresh SAW was better represented (R = 0.6 for salinity beyond 20 km).

Several significant events that are apparent in observations are also represented in the model fields (Fig. 3). Both series clearly show the 2017/2018 marine heatwave (Salinger et al., 2019), although the temperature maximum is underestimated (observations were 1.3 C warmer across transect on average) in the corresponding model temperature (Fig. 3a,b). Similarly, several nearshore salinity depressions coinciding with the arrival of NW are visible in the model data, despite overestimating the nearshore salinity during these events (Fig. 3d,e).

3.2. Variability of the Clutha River plume

First, the north-south spatial variability of the Clutha River plume was evaluated by calculating the latitudinal average (0.25 bins) of dye concentration over the shelf (inshore of the 500 m isobath) and slope (within 50 km offshore of the 500 m isobath). Shelf dye averages show that the modelled river plume rarely moved south of the Clutha River mouth, being most intense (highest surface concentrations) immediately downstream (to the northeast) up to the Otago Peninsula (Fig. 4a). Individual spikes of dye north of the Otago Peninsula were clear in the shelf series, with average concentrations exceeding 2.5 g/kg from 45.5 S to 44 S.

Significant dye concentrations beyond the 500 m isobath were much less frequent in the time series, rarely being visible due to small concentrations and short-lived nature (Fig. 4b). Dye most frequently crossed the 500 m isboath north of the 45 parallel, with slope concentrations south of the Otago Peninsula generally near zero. However, occasional crossing events near the Clutha River mouth can be seen (particularly between 2010 and 2011).

To consider the Clutha River plume on a finer spatial and temporal extent than seen in the shelf/slope time series, a series of three case studies were generated (Figs. 5, 6, 7). The case studies depict three distinct 10-day periods where mean dye concentrations beyond the shelf break were highest (black dots, Fig. 4). Over these 10-day windows, patterns in Q, τ_a, cross-isobath export, dye, SST, salinity,

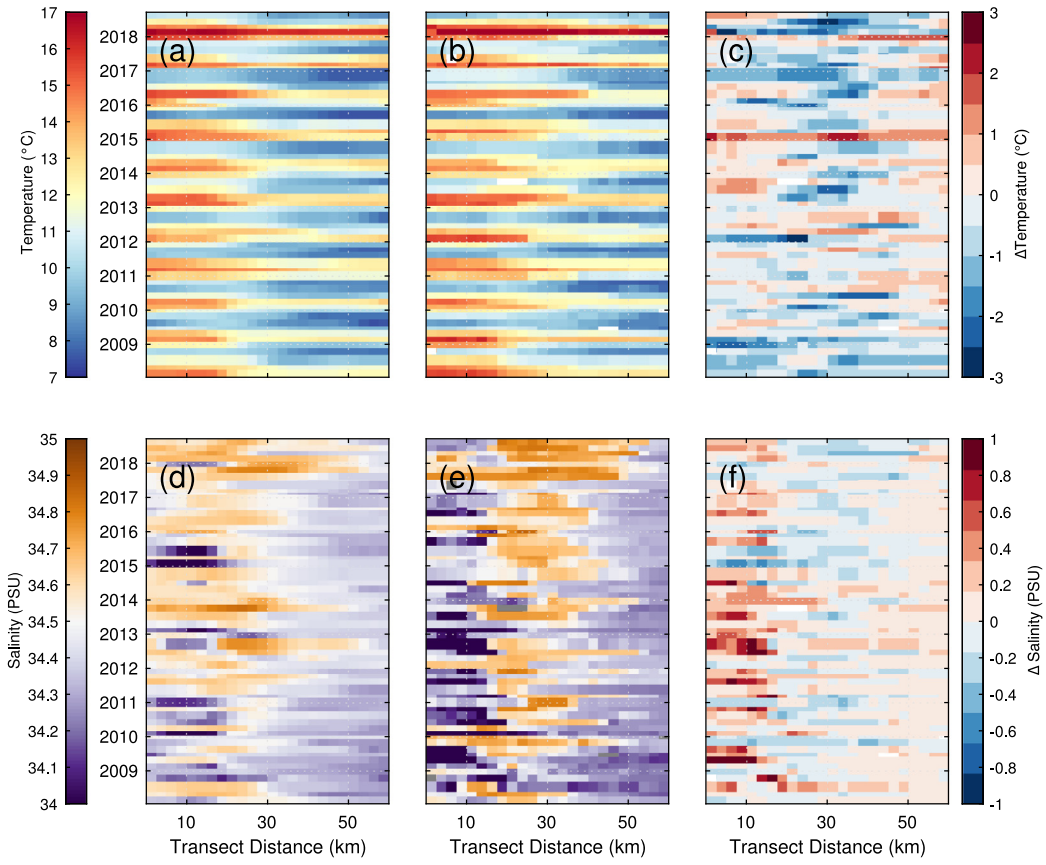

Fig. 3. Surface ROMS (a,d), *in situ* (b,e) temperature (top) and salinity (bottom) Hovmöller diagrams along the Munida Transect, and the difference between ROMS and *in situ* observations (c,f).

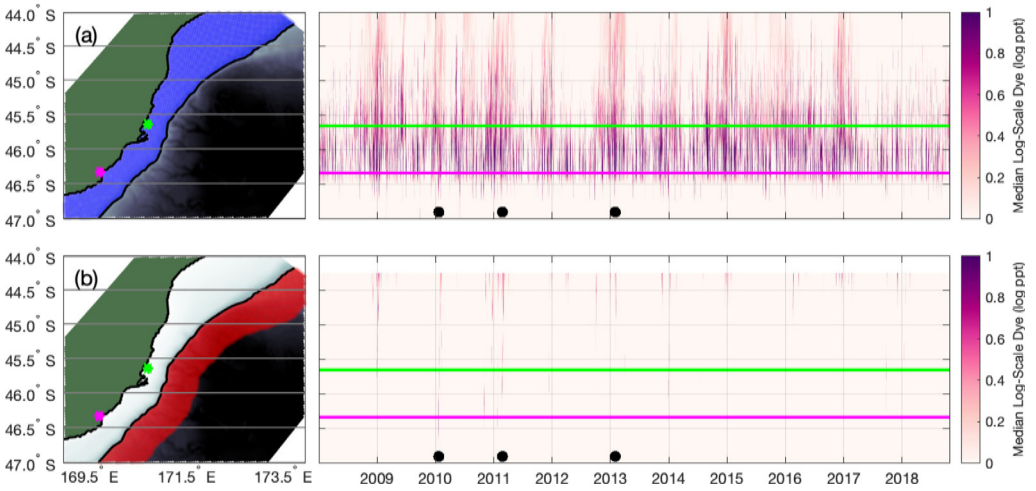

Fig. 4. Time series of median shelf (blue shaded area), (a), and slope (red shaded area), (b), log-scaled surface dye concentrations. Magenta dot (line, right panel) indicates the mouth of the Clutha River, green dot (line, right panel) indicates the north edge of the Otago Peninsula. Black dots indicate the timing of case studies.

Table 1
Table summarising mean Q, τ_a, wind speed (v_w), and wind direction during each case study, and ten days prior (preceding means are in brackets).

Case study	Duration	$\overline{Q}$ m^3/s)	$\overline{\tau_a}$ N/m^2)	$\overline{v_w}$ m/s)	Wind direction
1 (Fig. 5)	15/1/2010–25/1/2010	727 (812)	−0.01 (0.05)	6.2 (7.6)	ENE (WSW)
2 (Fig. 6)	18/2/2011–28/2/2011	731 (1163)	−0.03 (−0.02)	5.5 (6.0)	NE (NNE)
3 (Fig. 7)	25/1/2013–04/02/2013	651 (1059)	−0.03 (0.01)	5.1 (5.9)	NNE (WNW)

and circulation are considered (case study conditions are described in Table 1).

The first case study (Fig. 5) depicts a clear upfront/downfront wind shift occurring between January 15th and January 25th, 2010. Through

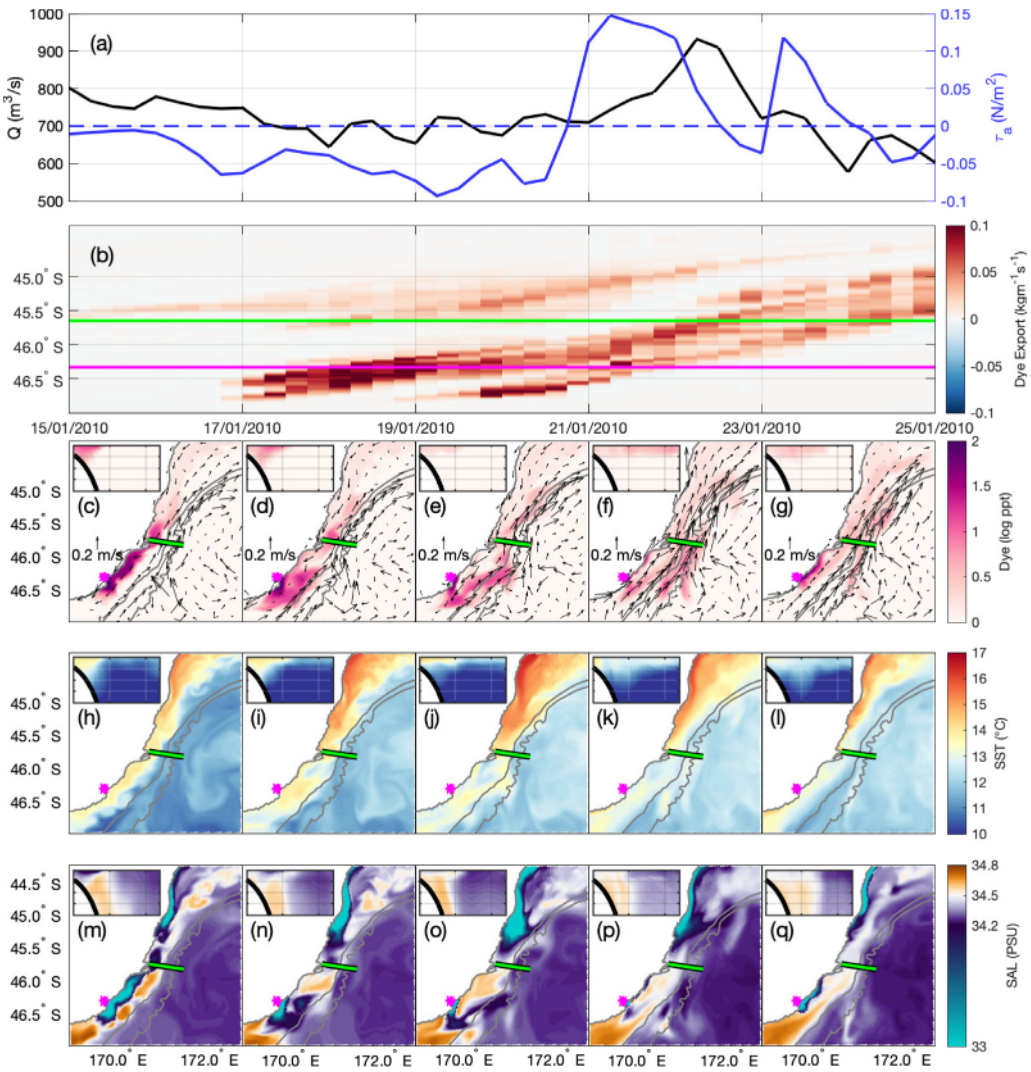

Fig. 5. Evolution of model fields during Case Study 1, spanning January 15th–25th, 2010. Time series of Q (black) and τ_a (blue), (a). Time series of dye export normal to the 500 m isobath, (b). Magenta line indicates the latitude of the mouth of the Clutha River, green line indicates the northern latitude of the Otago Peninsula. Two-day median surface dye concentration over the event (c-g). Black arrows show mean velocities in the upper 45 m. Two-day median SST over the event, (h–l). Two-day median cross-shelf salinity (m–q). The 1000 m and 500 m isobaths are contoured in grey. Insets depict cross-shelf depth structure of each field at the transect indicated in green. Grid lines show 25 m increments in vertical and 25 km increments in horizontal.

this period, Q was high relative to the January median (case study median 727 m^3s^{-1}, vs January median of 550 m^3s^{-1}). On January 15th–16th the nearshore salinity minimum and peak dye concentration was coastally constrained (Fig. 5c,m) and τ_a was becoming more negative (more upfront) (Fig. 5a). During this time, dye concentrations along the shelf became progressively more detached from the coast and began to cross the 500 m isobath north of the Otago Peninsula (Fig. 5b,c). By the 18th of January nearshore shelf currents deflected southwest (Fig. 5d) as northeasterly winds strengthened, accompanied by strong cross-isobath dye export south of the Clutha River mouth (Fig. 5b). As this event progresses, thermal stratification builds over the shelf break (Fig. 5h–l), coinciding with the spreading of dye and low salinity over the upper 25 m. In the final four days of the event (January 21st–25th), the τ_a reversed and turned downfront, with currents over the shelf resuming characteristic northeastward flow (Fig. 5f,g). The nearfield river plume becomes coastally constrained once more and cross isobath dye export decreases, shifting progressively northward (at a rate of roughly 0.4 m/s) as the plume is advected alongshore (Fig. 5b).

The second case study (Fig. 6), spanning February 18th to February 28th, 2011, depicts the time leading up to the largest off-shelf dye concentrations in the model run. Six days prior to the beginning of this case study, Q peaked at 1800 m^3s^{-1} (the largest flood of the ROMS simulation), leading to initially high dye concentrations over the shelf (Fig. 6c). Through the case study, Q remained relatively high (median 731 m^3s^{-1} vs February median of 493 m^3s^{-1}). Periods of strong upfront wind stress on February 19th coincide with a current reversal over the inner shelf (Fig. 6d), flowing to the southwest and causing nearshore NW to detach from the coast and move off-shelf into SAW (Fig. 6b,d,i,n). Winds generally shift lightly downfront from February 21st onward, and shelf currents resume flow to the northeast (Fig. 6e–g). The deflected Clutha plume is advected past the transect (green line, Fig. 6e) by the Southland Current, and cross-isobath dye export similarly decreases and moves northward with the plume (Fig. 6b).

The third case study (Fig. 7), depicting ROMS fields from January 25th to February 4th, 2013, is marked by large surface dye concentrations and strong thermal stratification. This event was preceded by significant (exceeding 1200 m^3s^{-1}) and slowly declining Q in the two weeks prior to the beginning of the case study. Wind stress was initially upfront (Fig. 7a) and shifted to near zero for the majority of the event. During this period of upfront stress, the shelf current was slowed/reversed, causing the Clutha Plume to reach the 500 m isobath (Fig. 7b,c,m). Thermal stratification over the shelf grows rapidly, creating strongly stratified conditions in the upper 25 m (Fig. 7i-l). Neritic

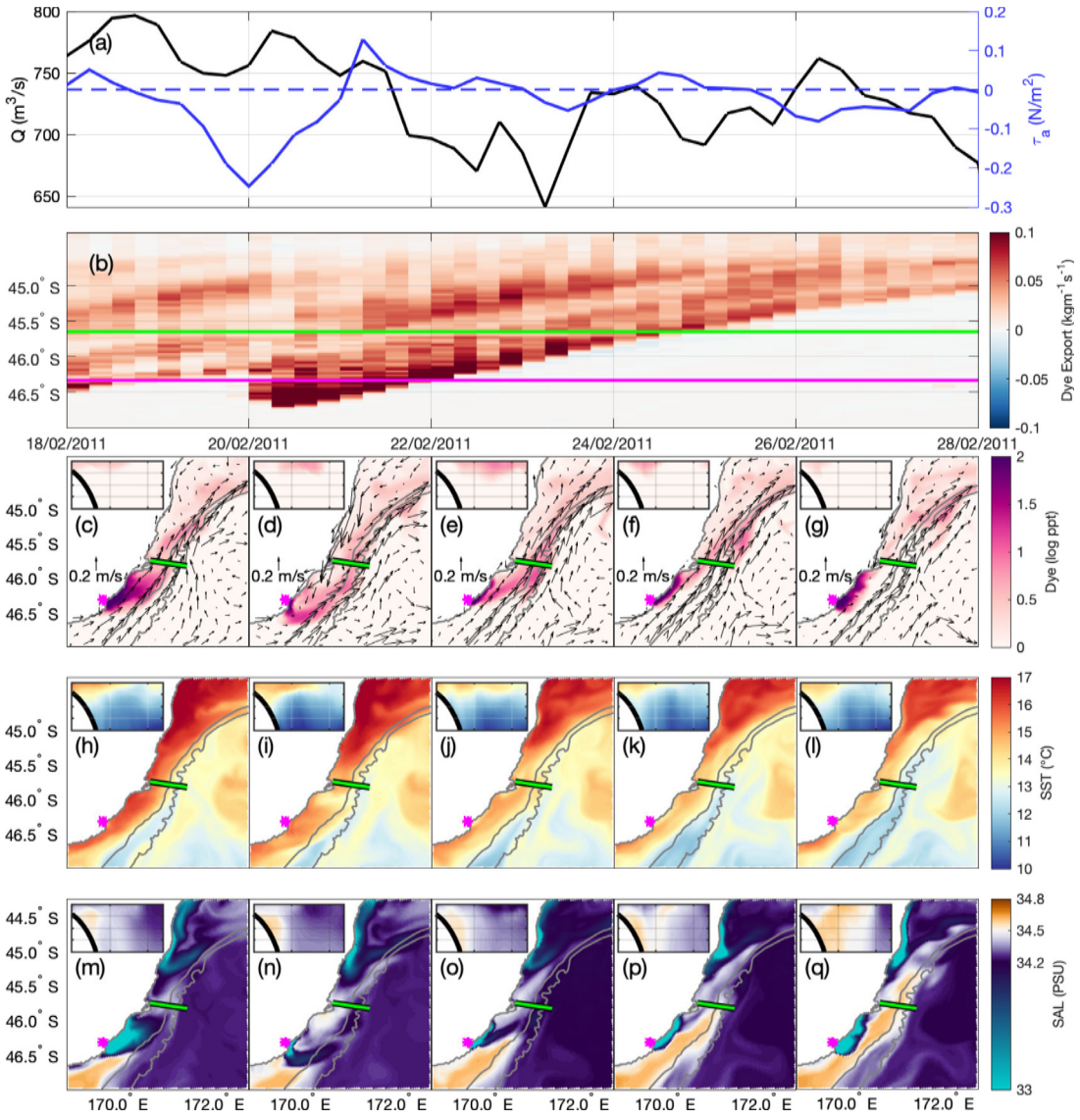

Fig. 6. Same as Fig. 5, for Case Study 2, spanning February 18th to February 28th, 2011.

water over the shelf is similarly apparent in the upper 25 m (Fig. 7m–q), spreading over the shelf and advecting northward. The low salinity surface signal of NW is particularly pronounced in this case study, even as it is advected northward.

3.3. Surface dye EOFs

Though the previous latitude-averaged time series provides insight into the downstream distribution of the Clutha River plume, the cross-shelf spatial structure of these responses is unclear. To investigate the dominant spatial patterns of plume variability, an EOF analysis was first performed on the seasonally-detrended log-scaled surface dye concentrations. Focus is given to the first two EOF modes, explaining a total 42.1 of anomalous dye concentration variability, as they were the most significant (according to the North Test, see Appendix Fig. A.14). The first mode shows a single-signed pattern over the mid-shelf, explaining 27.1 of overall variance (Fig. 8a). Regionally, the majority of the variance explained by this mode is in the near-field, accounting for 50 –70 of the variance over the mid-shelf immediately downstream of the Clutha River mouth, and decreasing in contribution beyond the Otago Peninsula (Fig. 8b). The PC time series of this mode was then compared against both Q anomaly and τ_a using composites. Correlation analysis of the PC time series with Q and τ_a show weak correlation, so we conditionally average the PC by Q and τ_a anomalies. Five bins of Q and τ_a anomaly are chosen to sub-sample and estimate averages, medians and inter-quartile ranges of each PC amplitude. A relationship between the PC and CRD and winds is clarified by these binned PC distributions (Fig. 8c,d). The median PC for periods of anomalously low discharge were negative, indicating negative dye anomalies over the mid-shelf, particularly in the near-field, when Q rates were low (Fig. 8c). Anomalously high discharge events (Q anomalies > 500 m^3s^{-1}) had a positive median PC, indicating an intensification of this pattern associated with high flow. PC distributions were more distinct when composited by τ_a (Fig. 8d). Intensifying downfront wind stress was associated with negative PCs, and light upfront wind stress anomalies were associated with positive PCs, suggesting a negative relationship between dye anomalies over the mid-shelf and downfront wind stress. However, strong upfront wind stress was associated with negative PCs as well, indicating that this mode weakens during intense upfront events. The correlation between the PC and Q anomaly was weak but significant (R = 0.13, p 0.01), whereas the correlation against τ_a was stronger (R = –0.36, p 0.01). In general, these results indicate that the first EOF mode intensifies with increased Q at zero lag, but responds more strongly to τ_a (weakening when winds become more downfront, Fig. 8d).

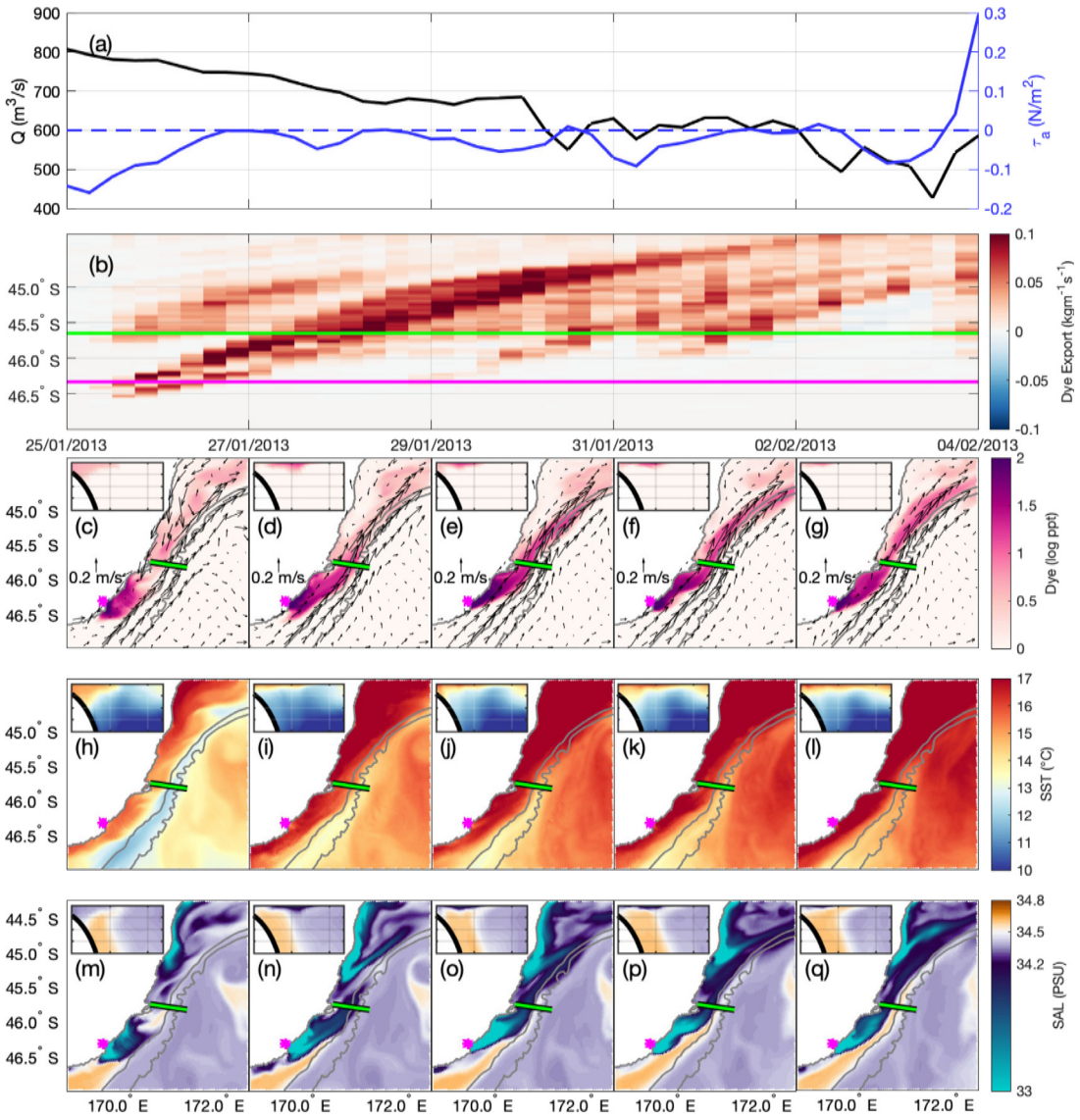

Fig. 7. Same as Fig. 5, for Case Study 3, spanning January 25th to February 4th, 2013.

The second EOF mode more closely resembled the patterns expected in response to upwelling/downfront wind stress (Choi and Wilkin, 2007) (Fig. 9a). When the PC time series of this mode is positive, there is a reduction in dye concentration over the mid-outer shelf and an intensification in the near shore. When the PC is negative, there are greater dye concentrations towards the shelf break immediately offshore of the Clutha River mouth. This EOF mode explains less total domain-wide variability than the first (16.6 , Fig. 9b), but represents over 50 of the local variability against the south coast of the Otago Peninsula. Binned PC time series distributions generally appear more linearly related to anomalous Q and τ_a than for the first mode (Fig. 9c,d). Anomalously high discharge is associated with increased dye concentration along the south coast of the Otago Peninsula, and over the mid-shelf further downstream. Low Q is associated with increased dye concentrations immediately offshore of the river mouth (Fig. 9c). Downfront wind stress (positive τ_a) generally strengthens dye concentrations against the coast downstream, and upfront wind stress (negative τ_a) increases dye concentrations offshore of the Clutha River mouth, towards the outer shelf (Fig. 9d). Correlation between the PC and Q anomaly was stronger for this mode (R = 0.20, p 0.01) than the first, whereas correlation between the PC and τ_a was weaker for this mode (R = 0.19, p 0.01).

3.4. Lagged correlations

The previous EOF analyses (Figs. 8 and 9) do not take into account potential temporal lags in dye advection along the shelf, or spin-up time of Ekman transport. This may contribute to relatively weak correlations between the PC time series and Q or τ_a. To evaluate the magnitude and timescales of plume response along the shelf, lagged correlations of surface dye concentrations (Fig. 10) against Q and τ_a were computed at each grid point.

Lagged correlations showed that anomalously high dye concentrations over the entire study region were associated with increased Q, increasing in lag moving downstream (Fig. 10a,b). Peak dye correlation to Q anomaly occurred immediately in front of the Clutha River mouth (R=0.6), and strong correlation values continued downstream in a band 20 km from the coast. There was a sharp increase in the lag of peak dye/Q correlation offshore of the 500 m isobath, and in the coastal area north of 44.5 S.

In general, correlations between anomalous dye concentrations and τ_a occurred at much shorter lags than against Q anomalies, with peak correlation at 2-day lag for most of the study region (Fig. 10d). Correlations between surface dye and τ_a were positive against most of the coast, particularly north of the Otago Peninsula, indicating that

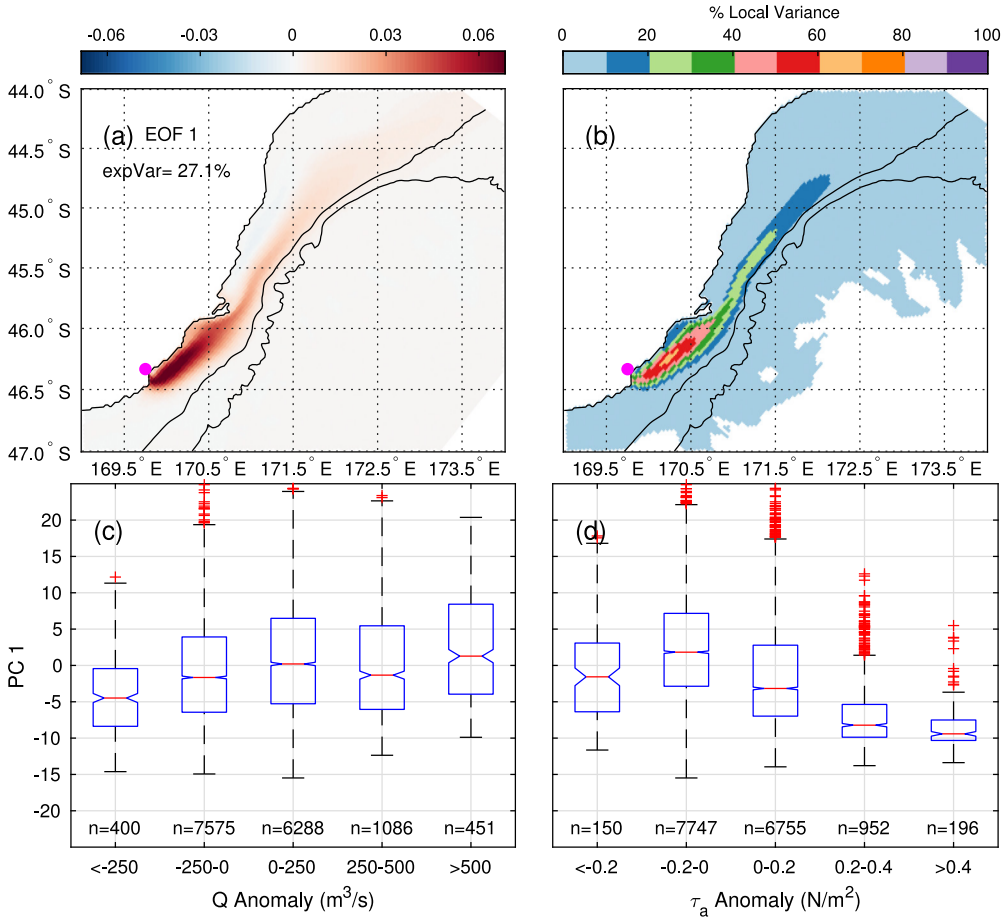

Fig. 8. (a), First EOF mode of seasonally-detrended log-scaled dye concentration. (b), Explained percentage of grid-cell dye anomaly variance. The 250, 500, and 1000 m isobaths are contoured in black. (c), Distributions of the principal component time series by binned Q anomaly. (d), Distributions of the principal component time series by binned τ_a anomaly (positive along-front wind is downfront).

increased downfront wind stress was associated with greater surface dye concentrations (Fig. 10c). The correlation between surface dye and τ_a was negative immediately adjacent to the Clutha River mouth, and over the outer shelf/slope further downstream, suggesting a relationship between increasing upfront wind stress and elevated surface dye concentrations (Fig. 10c).

3.5. Composite analysis

The coupled effects of Q and τ_a on spatial patterns of the Clutha River plume were investigated via composites of surface dye concentration anomalies with respect to both Q and τ_a (Fig. 11). Following the lags suggested by Fig. 10, the Q and τ_a anomalies were averaged over the preceding 9 and 3 days, respectively, before selecting events below/above the 25th/75th percentile.

For composites reflecting periods of anomalous upfront τ_a (Fig. 11a,d,g), surface dye concentration is generally reduced in the nearshore and increased offshore. As Q increases, offshore dye concentrations become more intense, and the nearshore negative anomaly weakens. Within the upfront composites, elevated dye concentrations only approached the shelf break downstream of the Otago Peninsula, and only during strong flow events (Fig. 11g). For median and strong Q (Fig. 11d,g), positive dye anomalies following upfront winds were clearly detached from the coast just beyond the Otago Peninsula (green transect) and limited to the upper 20 m of the water column.

For composites generated from periods where winds are within interquartile range of τ_a anomaly ("median wind"), surface dye concentration anomalies were generally less intense, and showed an increase downstream of the Clutha River as Q became stronger (Fig. 11b,e,h). Unlike the upfront wind composites, dye anomalies along the transect are more uniform through the water column following median wind events, exhibiting more of a coastally constrained structure.

Finally, composites formed during periods of downfront τ_a show strongly reduced surface dye concentrations over the mid-shelf (Fig. 11c,f,i). During downfront wind stress and weak Q, surface dye concentrations are reduced over the whole domain (Fig. 11c). As Q becomes stronger, surface dye concentrations increase close to the coast, both immediately south of the Otago Peninsula and downstream of it (Fig. 11f,i). Shoreward dye concentrations along the transect show positive anomalies at depth for all downfront wind composites (insets Fig. 11c,f,i), indicating that downfront wind stress is associated with mixing the dye through the water column. This consequentially weakens surface dye anomalies following downfront winds relative to the surface-limited plume structure observed following upfront wind stress.

These composites also show a notable impact of τ_a on the surface current over the shelf. During upfront winds, the current over the shelf generally slows by 10 cm/s, whereas it accelerates by 15 cm/s during downfront wind stress. Off-shelf, small cross-shelf velocity anomalies ($\pm$ 1 cm s^{-1}) consistent with the predicted direction of Ekman transport are apparent during composites corresponding to periods of upfront and downfront τ_a.

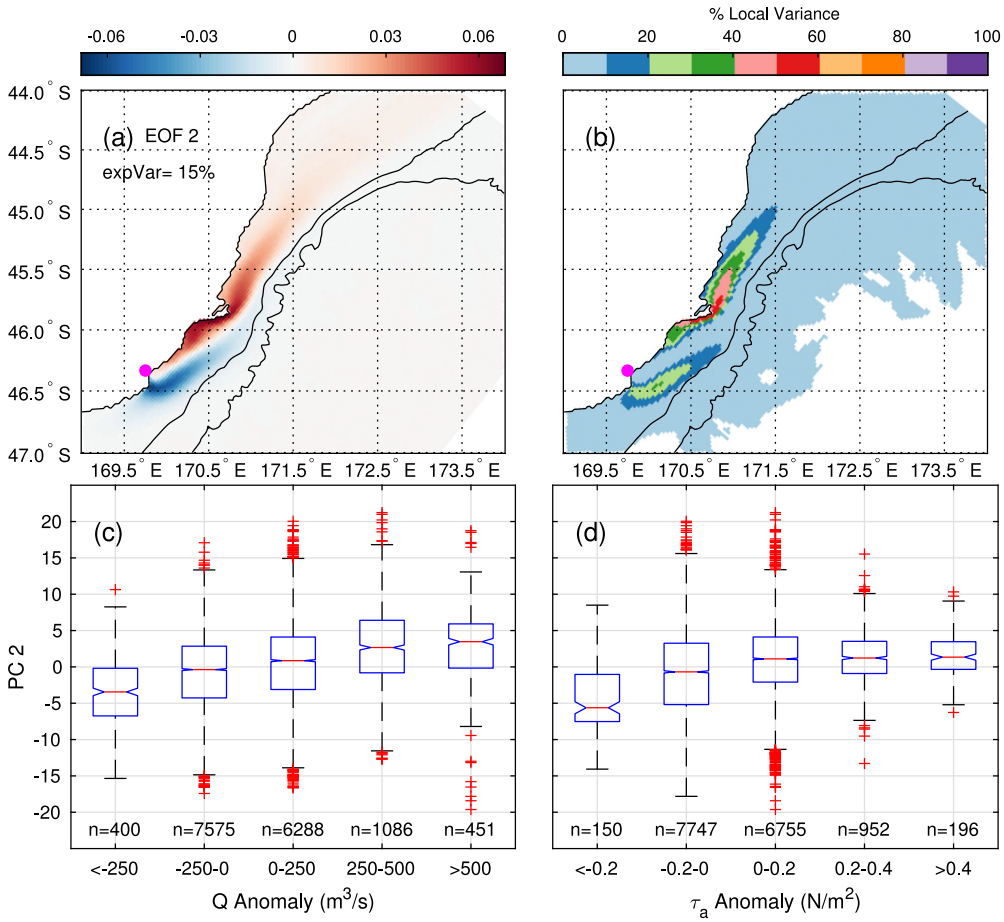

Fig. 9. (a), Second EOF mode of seasonally-detrended log-scaled dye concentration. (b), Explained percentage of grid-cell dye anomaly variance. The 250, 500, and 1000 m isobaths are contoured in black. (c), Distributions of the principal component time series by binned Q anomaly. (d), Distributions of the principal component time series by binned τ_a anomaly (positive along-front wind is downfront).

4. Discussion

4.1. Generalised plume structures

Previous studies in ANZ have established the role of Clutha River discharge in modifying the nearshore salinity of the Otago Shelf (Jillett, 1969; Hawke, 1992; Murdoch et al., 1990; Jones et al., 2013). However, the coarse spatiotemporal resolution of boat-based transects prohibited investigation of the evolution, variability, and drivers of the Clutha River plume as it moves downstream over the southeast shelf. This work presents the first efforts to characterise the Clutha River plume variability and its potential drivers. The analyses suggest a highly dynamic river plume that is responsive to changes in freshwater discharge, wind stress and currents. Three generalised plume structures evident from the present study are depicted in Fig. 12. The first panel depicts the general plume structure during periods of downfront wind stress (Fig. 12a). In this case, bulge formation at the river mouth is restricted by strong along-shelf currents and onshore Ekman transport.

The second panel shows a generalised response to initial/weak upfront wind stress (Fig. 12c), in which along-front currents weaken over the shelf and offshore Ekman transport moves the plume towards the shelf break. The plume shoals and disperses, spreading over a shallow surface layer. This constraining/offshore spreading of the plume against the coast in response to downfront/upfront wind stress is consistent with work in other coastal systems (Choi and Wilkin, 2007; Hickey et al., 2009; Warrick and Stevens, 2011; Moffat and Lentz, 2012; Kakoulaki et al., 2014; Fernández-Nóvoa et al., 2017), and is strongly supported by model results presented here through event depictions (Figs. 5, 6, and 7), EOFs (Figs. 8 and 9), and τ_a composites (Fig. 11).

The final panel illustrates a potentially novel plume structure for narrow shelf systems; wherein a nearshore current reversal detaches the plume from the coast, causing it to cross the continental shelf and shelf break and join with the frontal current (Fig. 12e). This mode resulted in the highest off-shelf dye concentrations throughout the model run, with a relatively concentrated stream of neritic water apparent off-shelf in each of the three events depicted (Figs. 5,6,7). Regions where freshwater plumes interact with the open ocean beyond the shelf break are generally limited to systems with large river discharge (>10,000 m^3s^{-1}) (Sharples et al., 2017; Schiller et al., 2011; Matano et al., 2014; Saldías et al., 2016), and/or interactions with offshore mesoscale eddies (Li et al., 2022; Schiller et al., 2011; Malauene et al., 2018). In contrast, the freshwater export considered in this work is generated by a comparatively modest river discharge of 1000 m^3s^{-1}, and is not associated with off-shelf eddies, underscoring its uniqueness in a field dominated by studies of significantly larger systems.

Each plume structure shown in the schematic is accompanied by true colour Sentinel II L2 A imagery of the shelf system during periods where low cloud cover and high sediment load allow for the visual identification of the plume. Each image was selected due to its resemblance to the described plume structures, and mean Q (over the preceding 4 days) and wind velocities over the previous 48 h were calculated. The observed winds show agreement with the predicted winds for each mode, and the Q is near seasonal medians (except for Fig. 12f, which is 250 m^3s^{-1} above the September median). Due to frequent cloud cover, and periods of low-sediment load inhibiting visual identification of the plume, analysis of a full colour-imagery data set was not pursued here. These images provide observational context to model results and the generalisations described.

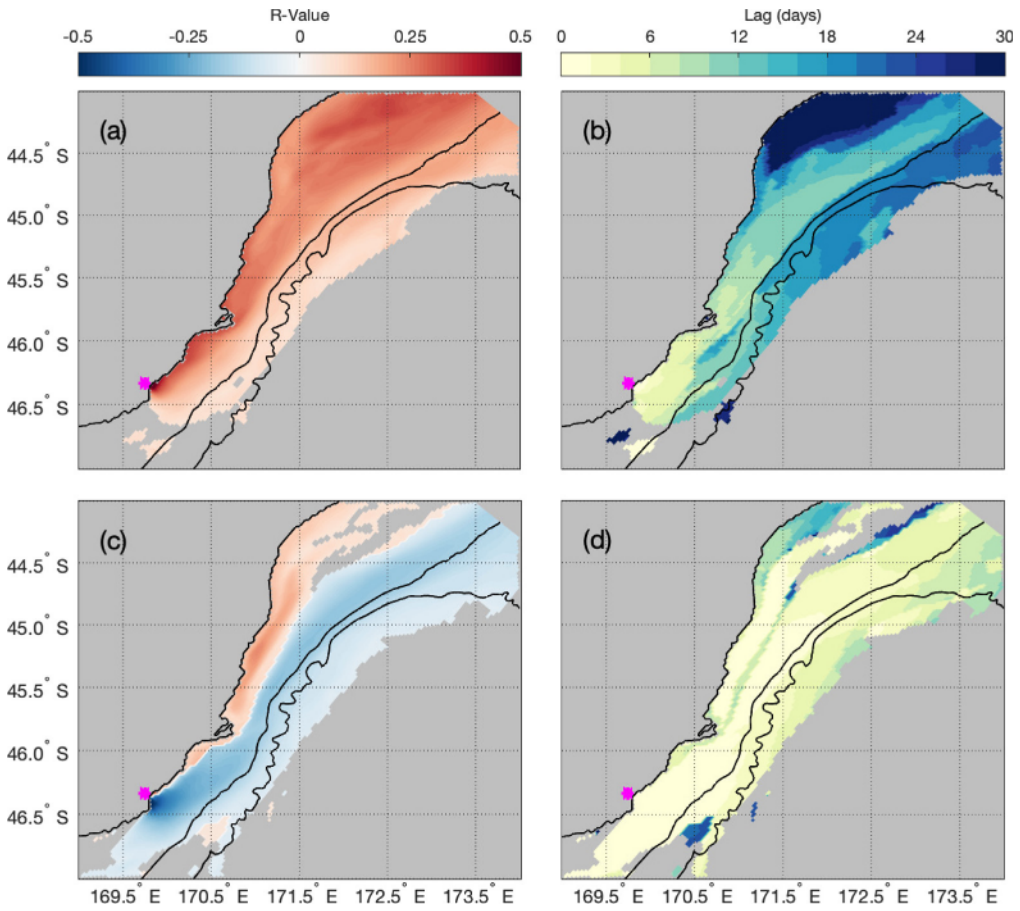

Fig. 10. Maximum Pearson's R-values for lagged correlations between surface dye anomaly and Q anomaly (a), and τ_a anomaly (c). Optimal lag between dye anomaly and Q anomaly (b), and τ_a anomaly (d). Magenta dot indicates the Clutha River mouth, 500 and 1000 m isobaths are indicated by black contours. Correlations not significant at 99 confidence intervals are filtered.

4.2. Regional implications

This work puts forward a mechanistic explanation for NW input beyond the shelf break. Previous *in situ* water sampling over the south-east ANZ continental shelf indicates that NW and neritic-modified STW are relatively rich in macro- and micro-nutrients such as iron, and silicate (Croot and Hunter, 1998; Currie et al., 2011; Baltar et al., 2015; Durante et al., 2021), the transport of which beyond the shelf break can support phytoplankton blooms in the High-Nutrient Low-Chlorophyll (HNLC) conditions in offshore SAW (Murphy et al., 2001; Boyd et al., 2004; Jones et al., 2013; Baltar et al., 2015). Silicate, which may be co-limiting with iron in SAW, has been shown to deplete coincidentally with elevated chlorophyll-a concentrations (Jones et al., 2013), suggesting that plume interactions beyond the shelf edge may play a role in the episodic blooms observed in offshore waters (Murphy et al., 2001; Boyd et al., 2004). Due to the relatively rare occurrence of offshore plume extent in model results (Fig. 4), *in situ* observations of such an event are likely challenging to capture.

Hawke (1992) first highlighted the short-term variability of nearshore salinity in this region. Throughout several repeat transects, distinct low-salinity pulses and complex surface structures were observed hours apart. An explicit connection was made between the detection of local minima in salinity and Q 4–12 days prior, consistent with the 6–8 day lag for peak dye-Q correlation observed off the Otago Peninsula in this study (Section 3.4b). Hawke (1992) further suggested that wind forcing and Southland Current variability played a factor in the structure observed. For example, observations made on March 5th 1987 were omitted from the salinity minimum correlation on account of "atypical water column structure", following a period of downfront wind stress (Hawke, 1992). Results from this study indicate that downfront wind stress can generate anomalously high dye concentrations against the coast off of the Otago Peninsula (*eg.* Fig. 12a), even during median Q, potentially accounting for the "anomalous" low-salinity observed by Hawke during this transect, and the coastally constrained isohaline structure. Frequently, Hawke observed salinity minimums slightly offshore of the coast. This pattern may be associated with coastal upwelling following upfront winds, moving the plume offshore and increasing salinity against the coast through upwelling of deep shelf/slope waters. This upwelling could also drive mixing that assists with dispersing the nearshore river plume (Bellafiore et al., 2019).

Previous work has also noted that the surface expression of STW over the mid to outer shelf is occasionally "capped" by a shallow surface layer of neritic water (Jillett, 1969; Croot and Hunter, 1998; Hopkins et al., 2010; Jones et al., 2013). This offshore spreading of neritic water is consistent with model results of plume response during weak/initial upfront wind stress. As CTD surveys of this coastline have generally been conducted on fair weather days, marked by reduced wind stress (Johnson et al., 2023), observations of nearshore constrained plumes (seemingly associated with strong southwesterly wind stress) may be underrepresented by historical CTD data. The stratification produced by freshwater plumes can also significantly increase rates of Ekman transport by reducing the thickness of the surface Ekman layer (Chen and Chen, 2017; García Berdeal, 2002). This in turn can influence the offshore advection of riverine nutrients, phytoplankton trapped in the river plume, and buoyancy along the shelf region (Hickey et al., 2010). An elevated rate of Ekman transport in a river plume could help further explain the rapid restratification observed at the front that borders the narrow SE continental shelf of NZ following upfront wind stress (Johnson et al., 2023).

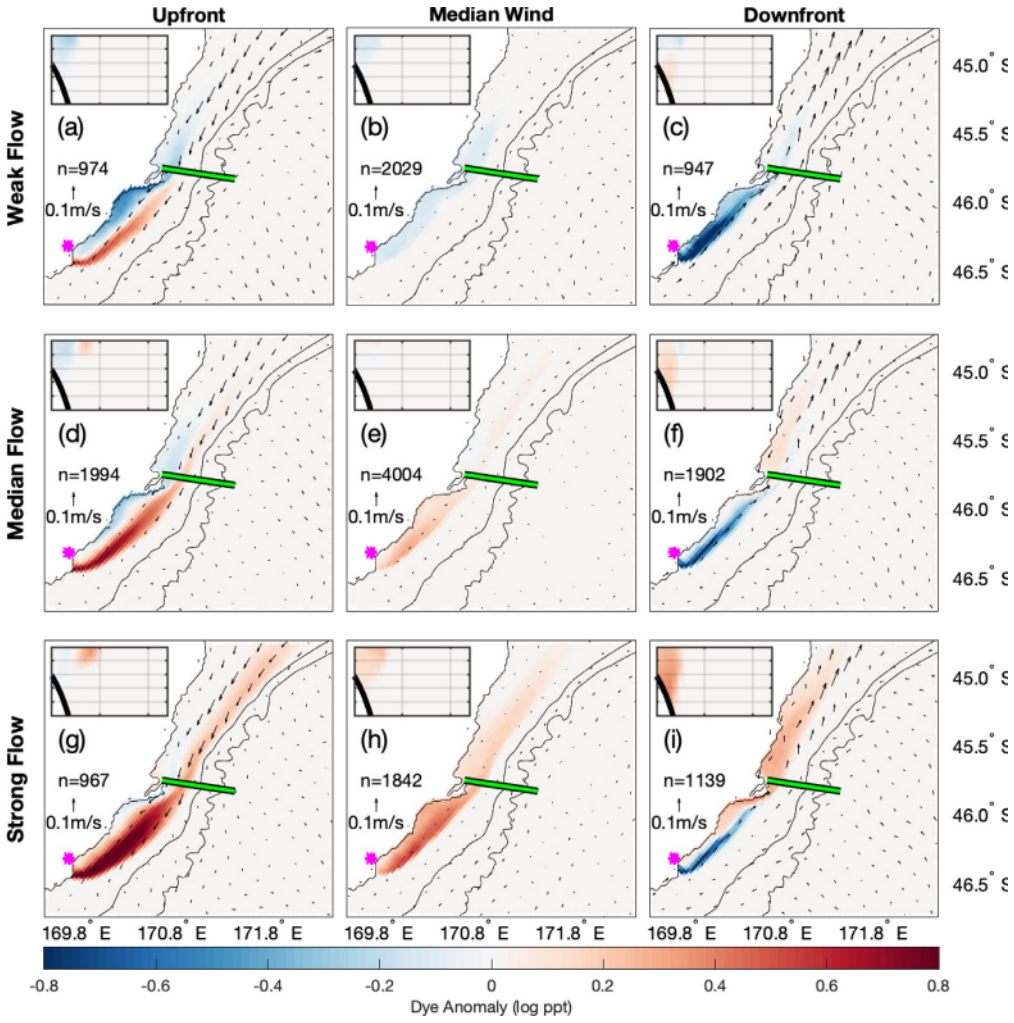

Fig. 11. Composites of log-scaled surface dye anomaly for upfront, median, and downfront wind stress (columns left to right) and weak, median, and strong Q anomaly (rows top to bottom). Current velocity anomalies in the upper 45 m are overlaid as black arrows. Insets depict dye anomaly at green transect. Grid lines show 10 m increments in vertical and 25 km increments in horizontal.

The relationship between the τ_a and modelled shelf current response has been previously identified in observations (Chiswell, 1996; Fernandez et al., 2018), and the model results support previous descriptions of a consistent northeast flow with extremely infrequent reversals over the shelf. From model results presented here, it appears that current velocities over the shelf (0–500 m depth) respond strongly to local wind forcing, with velocities offshore of the 500 m isobath relatively unaffected (Fig. 11). This finding is consistent with the work of Fernandez et al. (2018), who found that there was no correlation between Southland Current transport and local wind stress. This has potentially significant implications for mixing at the shelf edge, where shear between shelf and slope currents could generate 3-dimensional mixing (Brink, 2016; Krug et al., 2017; Taylor and Thompson, 2023) during periods where the flows over the shelf are slow or reversed relative to the Southland Current.

4.3. Implications for narrow shelf systems

Freshwater intrusion events can be significant drivers of nutrient fluxes and the associated phytoplankton variability at and across shelf break frontal boundaries (García Berdeal, 2002; Schiller et al., 2011; Sharples et al., 2017). Such events have been identified in large river systems, such as the Mississippi (Schiller et al., 2011), and Columbia (Mazzini et al., 2014; Saldías et al., 2016), but also in smaller river systems near relatively narrow continental shelves (*eg.* off the Iberian Peninsula; (Otero et al., 2008), or system considered in the present study; (Jones et al., 2013)). Depending upon the nutrient regime of shelf and slope waters, coastal detachment and off-shelf advection of river plumes via upfront wind stress may supply terrestrially derived limiting nutrients and generate episodic increases in Chl-a. The present study identified these deflection events as drivers of the largest off-shelf dye concentrations (Fig. 4b), associated with large depth-integrated dye export across the 500 m isobath (Figs. 5,6,7b). Accordingly, the sudden and relatively intense influx of nutrients driven by these plume deflection events can potentially stimulate localised, episodic phytoplankton blooms not captured by analysis at seasonal time scales.

In previous work that has attempted to quantify the proportion of riverine nutrients that reach the open ocean, Sharples et al. (2017) considered every shelf system on Earth. As a consequence of the study's global scale, generalisations were made for systems where the estimated plume width is narrower than the shelf break (such as the current system, as calculated in Section 1.2). On these narrow shelves, it was assumed that NW is completely dispersed through shelf waters before cross-shelf Ekman transport brings nutrients to the open ocean, and that their offshore transport can be approximated based on Ekman fluxes driven by annual mean wind stress. However, in the present work, off-shelf dye concentrations are shown to spike episodically on subseasonal time scales (Fig. 4b), as detached river plumes set up by positive river flow anomalies and upwelling-favourable wind stress. As

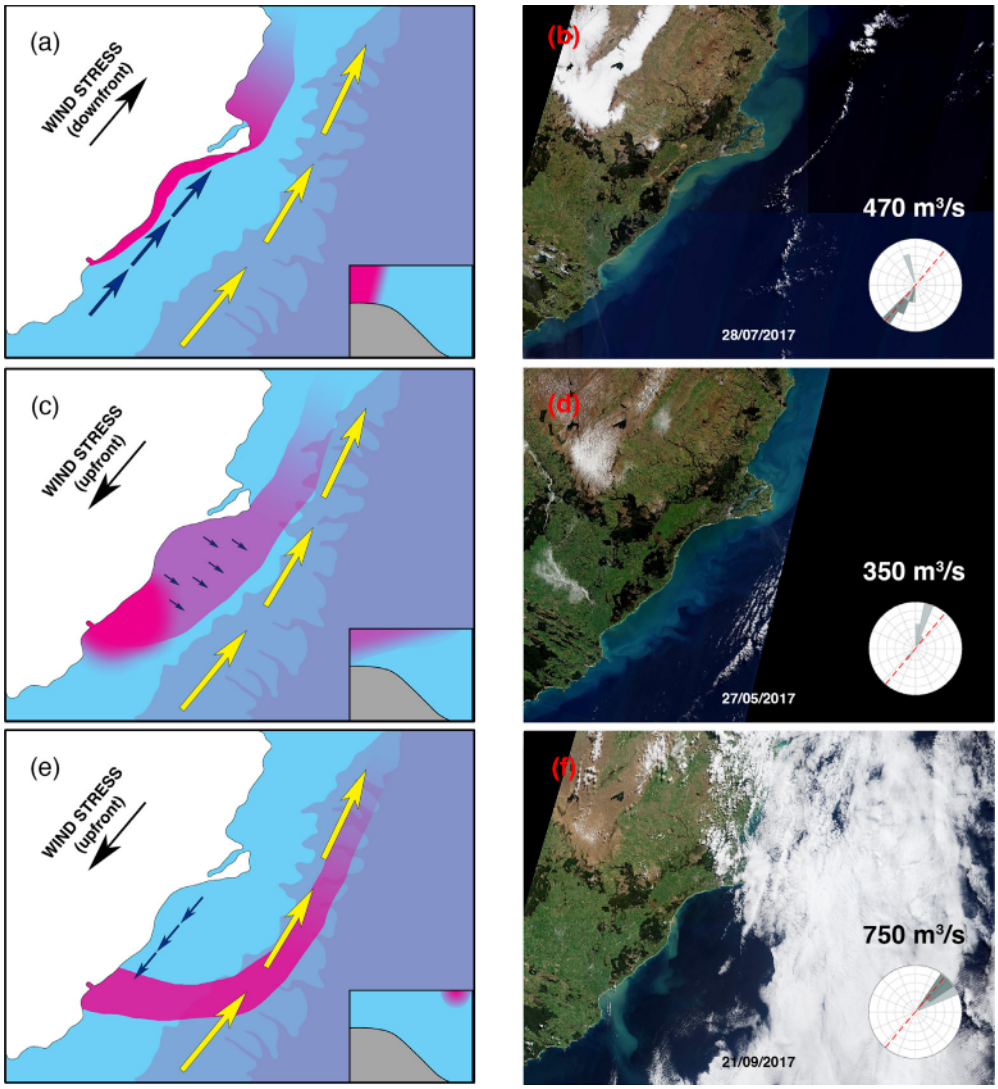

Fig. 12. Schematic diagram of three generalised plume structures. Magenta area represents the plume, blue arrows indicate simplified shelf flow, yellow arrows indicate Southland Current. Each schematic is complimented by Sentinel II L2 A true colour imagery reflecting the corresponding plume structure. Wind vectors in the preceding 48 h and mean Q over the 4 days prior are indicated.

a result, the most significant instances of cross-shelf nutrient transport at narrow shelves may only be accounted for when considering processes operating at subseasonal time scales rather than annual (Sharples et al., 2017). Although the intrusions of detached river plumes across a shelf-break front captured in the present work are short-lived, they occur over biologically relevant scales and the subsequent nutrient supply could contribute to anomalous bloom events around and beyond the shelf break at other narrow shelves globally (Jones et al., 2013).

In addition to the nutrients provided by freshwater discharge, buoyant river plumes also modify shelf stratification, affecting mixing depths and light availability for phytoplankton (Chen and Chen, 2017; García Berdeal, 2002; Hopkins et al., 2021; Masotti et al., 2018; Malan et al., 2024). Persistently elevated productivity near the river mouth of the Itata River in Central Chile has been suggested to be driven by both nutrient influx and stratification from the buoyant freshwater plume, particularly noticeable in winter when the shelf is otherwise weakly stratified (Testa et al., 2018). Elevated surface concentrations of Chl-a have also been observed over the southeast shelf of ANZ during winter months following periods of significant Clutha River flooding (Jones et al., 2013). Though the observed increases in Chl-a concentrations were primarily attributed to silicate replenishment from increased freshwater input (Jones et al., 2013), the shallow stratification created by a large river discharge event may also contribute to elevated Chl-a around shelf break fronts during well-mixed winter conditions. Under upfront wind stress conditions at narrow shelves, these buoyant waters may also advect beyond the shelf break and create episodic stratification events in the open ocean with implications for regional Chl-a dynamics. Both of these possibilities, which are demonstrated by the plume structures evident in the present work (e.g. Fig. 12), await further investigations.

4.4. Limitations and future work

One limitation in the model is an overestimation of nearshore salinity, and thus model results have reduced buoyancy of NW plumes downstream. The overestimation potentially reduces the magnitude of response to the forcings described in this work. As the model only represents historical discharge rates of the Clutha River, climatological forcing at the several smaller rivers along the model domain will not capture increased Q during flood events. The cumulative impact of these river flows likely generates a stronger nearshore NW band than represented in the model fields. Furthermore, nearshore salinities in this region are likely impacted by the advection of neritic-modified waters from the west coast of ANZ through the Foveaux Strait (Chiswell et al., 2015; Stevens et al., 2019), which are beyond the model domain.

The relative spatial coarseness of HYCOM data used at model boundaries likely does not capture the nearshore salinity depression due to significant river systems upstream of the model domain (Stevens et al., 2019), resulting in an overestimation of nearshore salinity at the western model boundary. Increased buoyancy of NW would be expected to intensify responses to wind and along-front currents (Choi and Wilkin, 2007; Hickey et al., 2010; da Silva and Castelao, 2018), so the general mechanisms modifying plume structure in the model are presumed to also act on a more-buoyant plume. Sensitivity analysis of the model to boundary conditions (HYCOM), and atmospheric forcing (NCEP/NCAR) would be highly beneficial for identifying sources of error in SST, salinity, and circulation between the model and observations. Additionally, in this simulation, only the Clutha River discharge is realistic, with other rivers constantly emitting annual mean discharge. Though the Clutha River is over ten times larger than all other rivers in this area combined, accurate flows for all regional rivers would contribute to increased nearshore buoyancy during flood conditions.

Understanding the impact and magnitude of the nutrient fluxes, represented passively by dye concentrations in this model, would require further consideration. Complex interactions between cross-frontal exchange, nutrient resuspension, and stratification likely generate a range of productivity responses in response to variable wind, riverine, and shelf-current drivers (Hickey et al., 2010; Fernández-Nóvoa et al., 2017; Masotti et al., 2018). The implementation and coupling of biogeochemical models with this model could shed more light on these interactions, and inform future observational work in the region.

A lack of fine-scale (daily, order of kilometers) spatiotemporal *in situ* data inhibits analysing observational examples of plume evolution as presented in this work. Many of the patterns described in this study cannot be resolved by any existing historical data from southeast ANZ, motivating the need for targeted, process-based experiments in this region. A cross-shelf mooring array outfitted with temperature and salinity loggers would allow the investigation of processes indicated in the model (such as offshore propagation and dispersion of low-salinity signals). Frequent repeat cross-shelf transects, akin to the work by Hawke (1992), would greatly improve the understanding of plume evolution, although weather and cost considerations make boat-based work of this scope unrealistic. Lastly, the satellite images included in Fig. 12 indicate a currently untapped observational record of plume evolution in this region. The utilisation of ocean-colour images to track river plumes (Dzwonkowski and Yan, 2005; Walker et al., 2005; Chant et al., 2008; Mazzini et al., 2014; Saldías et al., 2016) may offer insight into the patterns described when averaged over sufficiently long periods to overcome poor coverage due to cloud cover. Further observational data collection will also improve confidence in model-observation comparisons, as the Munida data set is biased towards odd-numbered months (being collected bi-monthly), and possibly over-represents hydrographic conditions during calm weather (Johnson et al., 2023).

Finally, future work is required to discern the role of southeast ANZ's geomorphology in generating the coastal circulation patterns described in the current study. Though previous idealised simulations of river plumes (Fong and Geyer, 2001) display coastal detachment and nearshore current reversals following upfront wind stress, the degree of coastal detachment observed in southeast ANZ may be intensified by the Otago Peninsula and headland north of the Clutha River (Murdoch et al., 1990; Warrick and Stevens, 2011).

5. Conclusions

Through a combination of event analysis, lagged correlations, EOFs, and composite analysis, numerical model results suggest a strong relationship between the plume over the Otago Shelf and river discharge, τ_a, and shelf current velocities. The arrival of NW at the shelf break appears to be linked to upfront wind stress and can do so through two generalised plume regimes. Upfront wind stress appears to first move river plumes offshore through Ekman transport, dispersing the plume over a shallow surface layer stretching over the shelf. Prolonged or intense upfront wind stress appears to generate a current reversal over the inner shelf that detaches the plume from the coast and deflects it off-shelf before being advected downstream by the Southland Current. This plume detachment mechanism could generate large nutrient fluxes into the open ocean for regions where the river plume width is comparable to the shelf width, potentially driving episodic increases in Chl-a at and beyond shelf break fronts. During downfront wind stress, the plume appears coastally constrained by on-shore Ekman transport and strong along-front flow, consistent with work in other systems. Robust validation of these model results requires fine-scale spatiotemporal observational data over the shelf region, but the novel results from this study offer an important first step to understanding the mechanisms underpinning subseasonal variability of the river plume in this globally unique region. Furthermore, for narrow shelf regions with significant freshwater discharge, characterisation of the plume response to along-shelf wind forcing at subseasonal scales should be undertaken to investigate how neritic water intrusions may affect productivity and nutrient fluxes at shelf break fronts.

CRediT authorship contribution statement

Erik E. Johnson: Conceptualization, Formal analysis, Investigation, Methodology, Visualization, Writing – original draft, Writing – review & editing. **Charine Collins:** Data curation, Methodology, Resources, Writing – original draft, Writing – review & editing. **Sutara H. Suanda:** Conceptualization, Supervision, Writing – review & editing. **Stephen R. Wing:** Conceptualization, Supervision, Writing – review & editing. **Kim I. Currie:** Data curation, Resources, Writing – review & editing. **Jesse Vance:** Conceptualization, Writing – review & editing. **Robert O. Smith:** Conceptualization, Funding acquisition, Methodology, Project administration, Supervision, Writing – review & editing.

Declaration of competing interest

The authors declare the following financial interests/personal relationships which may be considered as potential competing interests: Charine Collins reports financial support was provided by New Zealand Ministry of Business Innovaton and Employment. Kim Currie reports financial support was provided by Natonal Insttute of Water and Atmospheric Research. If there are other authors, they declare that they have no known competing financial interests or personal relationships that could have appeared to infuence the work reported in this paper.

Data availability

Data will be made available on request.

Acknowledgements

We'd like to acknowledge the crew of the Polaris II research vessel, Bill Dickson and Mark Elder, as well as staff and students who have contributed to the Munida Transect through the years. This work is supported by the NZ Tertiary Education PBRF and a University of Otago, New Zealand Ph.D. Scholarship to E.E.J. The Munida Transect is supported by SIFF funding from the National Institute of Water and Atmospheric Research (NIWA) and strategic funding from the University of Otago, New Zealand. Modelling was supported by SSIF funding from the New Zealand Ministry of Business, Innovation and Employment. Altimetry data used in this study (v2.1, https://DOI10.24400/527896/a01-2022.020) were developed, validated by the CTOH/LEGOS, France and distributed by Aviso+. Meteorological data used in this study (ERA5, https://doi.org/10.24381/cds.adbb2d47) were obtained from the Copernicus Climate Data Store. Model output can be requested from Dr Charine Collins (charine.collins@niwa.co.nz).

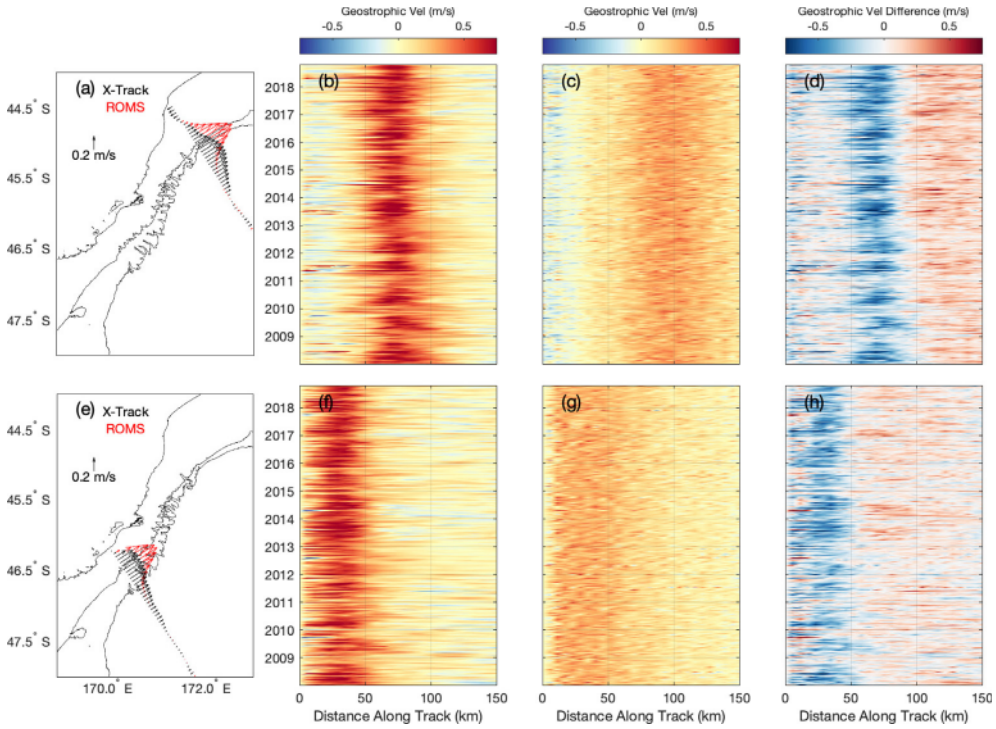

Fig. A.13. Position of mean geostrophic velocities (a,e), Hovmöller diagrams from ROMS (b,f) and X-Track (c,g), and X-Track-ROMS difference in geostrophic velocities (d,h) for altimetry tracks 188 (top) and 112 (bottom).

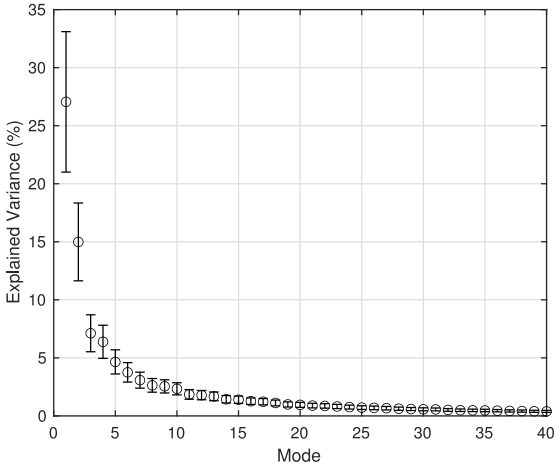

Fig. A.14. Explained variance and uncertainty (from North Test) for first 40 modes of seasonally detrended log-scaled dye EOF.

Appendix

Fig. A.13 depicts geostrophic velocities calculated from X-Track and ROMS along tracks 188 and 112. Generally, ROMS velocities (Fig. A.13b,f) are consistently higher than X-Track observations (Fig. A.13c,g). For track 188 (Fig. A.13, top row), the fastest part of the geostrophic current is located 25 km inshore of the peak current in observations.

Fig. A.14 shows a scree plot indicating the explained variance for the first 40 EOF modes of detrended, log-scaled surface dye concentrations. Uncertainties are indicated by error bars, calculated via the North Test (Loughran et al., 2017). As uncertainty does not overlap for the first two modes of the EOF, they are focused on in the analysis.

References

Augé, A., Lalas, C., Davis, L., Chilvers, B., 2012. Autumn diet of recolonising female New Zealand sea lions based at Otago Peninsula, South Island, New Zealand. New Zealand J. Marine Freshwater Res. 46 (1), 97–110. http://dx.doi.org/10.1080/00288330.2011.606326, URL http://www.tandfonline.com/doi/abs/10.1080/00288330.2011.606326.

Baltar, F., Stuck, E., Morales, S., Currie, K., 2015. Bacterioplankton carbon cycling along the subtropical frontal zone off New Zealand. Prog. Oceanogr. 135, 168–175. http://dx.doi.org/10.1016/j.pocean.2015.05.019, URL https://linkinghub.elsevier.com/retrieve/pii/S0079661115001160.

Bellafiore, D., Ferrarin, C., Braga, F., Zaggia, L., Maicu, F., Lorenzetti, G., Manfè, G., Brando, V., De Pascalis, F., 2019. Coastal mixing in multiple-mouth deltas: A case study in the Po delta, Italy. Estuar. Coast. Shelf Sci. 226, 106254. http://dx.doi.org/10.1016/j.ecss.2019.106254, URL https://linkinghub.elsevier.com/retrieve/pii/S0272771418309740.

Biggs, B.J.F., Duncan, M.J., Jowett, I.G., Quinn, J.M., Hickey, C.W., Davies-Colley, R.J., Close, M.E., 1990. Ecological characterisation, classification, and modelling of New Zealand rivers: An introduction and synthesis. New Zealand J. Marine Freshwater Res. 24 (3), 277–304. http://dx.doi.org/10.1080/00288330.1990.9516426, URL http://www.tandfonline.com/doi/abs/10.1080/00288330.1990.9516426.

Birol, F., Fuller, N., Lyard, F., Cancet, M., Niño, F., Delebecque, C., Fleury, S., Toublanc, F., Melet, A., Saraceno, M., Léger, F., 2017. Coastal applications from nadir altimetry: Example of the X-TRACK regional products. Adv. Space Res. 59 (4), 936–953. http://dx.doi.org/10.1016/j.asr.2016.11.005, URL https://linkinghub.elsevier.com/retrieve/pii/S0273117716306317.

Boyd, P.W., McTainsh, G., Sherlock, V., Richardson, K., Nichol, S., Ellwood, M., Frew, R., 2004. Episodic enhancement of phytoplankton stocks in New Zealand subantarctic waters: Contribution of atmospheric and oceanic iron supply: iron supply to subantarctic waters. Glob. Biogeochem. Cycles 18 (1), n/a–n/a. http://dx.doi.org/10.1029/2002GB002020, URL http://doi.wiley.com/10.1029/2002GB002020.

Brink, K., 2016. Cross-shelf exchange. Annual Rev. Marine Sci. 8 (1), 59–78. http://dx.doi.org/10.1146/annurev-marine-010814-015717, URL http://www.annualreviews.org/doi/10.1146/annurev-marine-010814-015717.

Chant, R.J., Glenn, S.M., Hunter, E., Kohut, J., Chen, R.F., Houghton, R.W., Bosch, J., Schofield, O., 2008. Bulge formation of a buoyant river outflow. J. Geophys. Res. 113 (C1), C01017. http://dx.doi.org/10.1029/2007JC004100, URL http://doi.wiley.com/10.1029/2007JC004100.

Chao, S.-Y., Boicourt, W.C., 1986. Onset of estuarine plumes. J. Phys. Oceanogr. 16 (12), 2137–2149. http://dx.doi.org/10.1175/1520-0485(1986)016<2137:OOEP>2.0.CO;2, URL http://journals.ametsoc.org/doi/10.1175/1520-0485(1986)016 3C2137:OOEP 3E2.0.CO;2.

Chassignet, E.P., Verron, J. (Eds.), 2006. Ocean weather forecasting: an integrated view of oceanography. Springer, Dordrecht, OCLC: 65579740.

Chen, S.-Y., Chen, S.-N., 2017. Generation of upwelling circulation under downwelling-favorable wind within bottom-attached, buoyant coastal currents. J. Phys. Oceanogr. 47 (10), 2499–2519. http://dx.doi.org/10.1175/JPO-D-16-0271.1, URL http://journals.ametsoc.org/doi/10.1175/JPO-D-16-0271.1.

Chiswell, S.M., 1996. Variability in the Southland Current, New Zealand. New Zealand J. Marine Freshwater Res. 30 (1), 1–17. http://dx.doi.org/10.1080/00288330.1996.9516693, URL http://www.tandfonline.com/doi/abs/10.1080/00288330.1996.9516693.

Chiswell, S.M., Bostock, H.C., Sutton, P.J., Williams, M.J., 2015. Physical oceanography of the deep seas around New Zealand: a review. New Zealand J. Marine Freshwater Res. 49 (2), 286–317. http://dx.doi.org/10.1080/00288330.2014.992918, URL http://www.tandfonline.com/doi/full/10.1080/00288330.2014.992918.

Choi, B.-J., Wilkin, J.L., 2007. The effect of wind on the dispersal of the hudson river plume. J. Phys. Oceanogr. 37 (7), 1878–1897. http://dx.doi.org/10.1175/JPO3081.1, URL http://journals.ametsoc.org/doi/abs/10.1175/JPO3081.1.

Croot, P.L., Hunter, K.A., 1998. Trace metal distributions across the continental shelf near Otago Peninsula, New Zealand. Mar. Chem. 62 (3–4), 185–201. http://dx.doi.org/10.1016/S0304-4203(98)00036-X, URL https://linkinghub.elsevier.com/retrieve/pii/S030442039800036X.

Currie, K.I., Reid, M.R., Hunter, K.A., 2011. Interannual variability of carbon dioxide drawdown by subantarctic surface water near New Zealand. Biogeochemistry 104 (1–3), 23–34. http://dx.doi.org/10.1007/s10533-009-9355-3, URL http://link.springer.com/10.1007/s10533-009-9355-3.

da Silva, C.E., Castelao, R.M., 2018. Mississippi river plume variability in the gulf of Mexico from SMAP and MODIS-aqua observations. J. Geophys. Res.: Oceans 123 (9), 6620–6638. http://dx.doi.org/10.1029/2018JC014159, URL http://doi.wiley.com/10.1029/2018JC014159.

Durante, L., Smith, R., Kolodzey, S., McMullin, R., Salmond, N., Schlieman, C., O'Connell-Milne, S., Frew, R., Van Hale, R., Wing, S., 2021. Oceanographic transport along frontal zones forms carbon, nitrogen, and oxygen isoscapes on the east coast of New Zealand: Implications for ecological studies. Cont. Shelf Res. 216, 104368. http://dx.doi.org/10.1016/j.csr.2021.104368, URL https://linkinghub.elsevier.com/retrieve/pii/S027843432100025X.

Dzwonkowski, B., Yan, X.-H., 2005. Tracking of a Chesapeake Bay estuarine outflow plume with satellite-based ocean color data. Cont. Shelf Res. 25 (16), 1942–1958. http://dx.doi.org/10.1016/j.csr.2005.06.011, URL https://linkinghub.elsevier.com/retrieve/pii/S027843430500124X.

Fernandez, D., Bowen, M., Sutton, P., 2018. Variability, coherence and forcing mechanisms in the New Zealand ocean boundary currents. Prog. Oceanogr. 165, 168–188. http://dx.doi.org/10.1016/j.pocean.2018.06.002, URL https://linkinghub.elsevier.com/retrieve/pii/S0079661117303440.

Fernández-Nóvoa, D., Gómez-Gesteira, M., Mendes, R., deCastro, M., Vaz, N., Dias, J.M., 2017. Influence of main forcing affecting the Tagus turbid plume under high river discharges using MODIS imagery. In: Magar, V. (Ed.), PLOS ONE 12 (10), e0187036. http://dx.doi.org/10.1371/journal.pone.0187036, URL https://dx.plos.org/10.1371/journal.pone.0187036.

Fong, D.A., Geyer, W.R., 2001. Response of a river plume during an upwelling favorable wind event. J. Geophys. Res.: Oceans 106 (C1), 1067–1084. http://dx.doi.org/10.1029/2000JC900134, URL https://agupubs.onlinelibrary.wiley.com/doi/10.1029/2000JC900134.

García Berdeal, I., 2002. Influence of wind stress and ambient flow on a high discharge river plume. J. Geophys. Res. 107 (C9), 3130. http://dx.doi.org/10.1029/2001JC000932, URL http://doi.wiley.com/10.1029/2001JC000932.

Greene, C.A., Thirumalai, K., Kearney, K.A., Delgado, J.M., Schwanghart, W., Wolfenbarger, N.S., Thyng, K.M., Gwyther, D.E., Gardner, A.S., Blankenship, D.D., 2019. The climate data toolbox for MATLAB. Geochem. Geophys. Geosyst. 20 (7), 3774–3781. http://dx.doi.org/10.1029/2019GC008392, URL https://onlinelibrary.wiley.com/doi/10.1029/2019GC008392.

Hawke, D.J., 1989. Hydrology and near-surface nutrient distribution along the South Otago continental shelf, New Zealand, in summer and winter 1986. New Zealand J. Marine Freshwater Res. 23 (3), 411–420. http://dx.doi.org/10.1080/00288330.1989.9516377, URL http://www.tandfonline.com/doi/abs/10.1080/00288330.1989.9516377.

Hawke, D.J., 1992. Salinity variability in shelf waters near Otago Peninsula, New Zealand, on a time scale of hours. New Zealand J. Marine Freshwater Res. 26 (2), 167–173. http://dx.doi.org/10.1080/00288330.1992.9516511, URL http://www.tandfonline.com/doi/abs/10.1080/00288330.1992.9516511.

Hawke, D., 1995. Reactive silicate in shelf waters near Otago Peninsula, New Zealand. Marine Freshwater Res. 46 (2), 427. http://dx.doi.org/10.1071/MF9950427, URL http://www.publish.csiro.au/?paper=MF9950427.

Haywood, G.J., 2004. Some effects of river discharges and currents on phytoplankton in the sea off Otago, New Zealand. New Zealand J. Marine Freshwater Res. 38 (1), 103–114. http://dx.doi.org/10.1080/00288330.2004.9517222, URL http://www.tandfonline.com/doi/abs/10.1080/00288330.2004.9517222.

Heath, R.A., 1972. The southland current. New Zealand J. Marine Freshwater Res. 6 (4), 497–533. http://dx.doi.org/10.1080/00288330.1972.9515444, URL http://www.tandfonline.com/doi/abs/10.1080/00288330.1972.9515444.

Hersbach, H., Bell, B., Berrisford, P., Hirahara, S., Horányi, A., Muñoz-Sabater, J., Nicolas, J., Peubey, C., Radu, R., Schepers, D., Simmons, A., Soci, C., Abdalla, S., Abellan, X., Balsamo, G., Bechtold, P., Biavati, G., Bidlot, J., Bonavita, M., Chiara, G., Dahlgren, P., Dee, D., Diamantakis, M., Dragani, R., Flemming, J., Forbes, R., Fuentes, M., Geer, A., Haimberger, L., Healy, S., Hogan, R.J., Hólm, E., Janisková, M., Keeley, S., Laloyaux, P., Lopez, P., Lupu, C., Radnoti, G., Rosnay, P., Rozum, I., Vamborg, F., Villaume, S., Thépaut, J.-N., 2020. The ERA5 global reanalysis. Q. J. R. Meteorol. Soc. 146 (730), 1999–2049. http://dx.doi.org/10.1002/qj.3803, URL https://onlinelibrary.wiley.com/doi/10.1002/qj.3803.

Hickey, B.M., Kudela, R.M., Nash, J.D., Bruland, K.W., Peterson, W.T., MacCready, P., Lessard, E.J., Jay, D.A., Banas, N.S., Baptista, A.M., Dever, E.P., Kosro, P.M., Kilcher, L.K., Horner-Devine, A.R., Zaron, E.D., McCabe, R.M., Peterson, J.O., Orton, P.M., Pan, J., Lohan, M.C., 2010. River influences on shelf ecosystems: Introduction and synthesis. J. Geophys. Res. 115, C00B17. http://dx.doi.org/10.1029/2009JC005452, URL http://doi.wiley.com/10.1029/2009JC005452.

Hickey, B., McCabe, R., Geier, S., Dever, E., Kachel, N., 2009. Three interacting freshwater plumes in the northern California current system. J. Geophys. Res. 114, C00B03. http://dx.doi.org/10.1029/2008JC004907, URL http://doi.wiley.com/10.1029/2008JC004907.

Hopkins, J., Palmer, M.R., Poulton, A.J., Hickman, A.E., Sharples, J., 2021. Control of a phytoplankton bloom by wind-driven vertical mixing and light availability. Limnol. Oceanogr. 66 (5), 1926–1949. http://dx.doi.org/10.1002/lno.11734, URL https://onlinelibrary.wiley.com/doi/10.1002/lno.11734.

Hopkins, J., Shaw, A., Challenor, P., 2010. The Southland front, New Zealand: Variability and ENSO correlations. Cont. Shelf Res. 30 (14), 1535–1548. http://dx.doi.org/10.1016/j.csr.2010.05.016, URL https://linkinghub.elsevier.com/retrieve/pii/S0278434310001937.

Horner-Devine, A.R., 2009. The bulge circulation in the Columbia river plume. Cont. Shelf Res. 29 (1), 234–251. http://dx.doi.org/10.1016/j.csr.2007.12.012, URL https://linkinghub.elsevier.com/retrieve/pii/S0278434307003354.

Jillett, J.B., 1969. Seasonal hydrology of waters off the Otago peninsula, South-Eastern New Zealand. New Zealand J. Marine Freshwater Res. 3 (3), 349–375. http://dx.doi.org/10.1080/00288330.1969.9515303, URL http://www.tandfonline.com/doi/abs/10.1080/00288330.1969.9515303.

Johnson, E.E., Suanda, S.H., Wing, S.R., Currie, K.I., Smith, R.O., 2023. Episodic summer chlorophyll-a blooms driven by along-front winds at aotearoa's Southeast shelf break front. J. Geophys. Res.: Oceans 128 (7), e2022JC019609. http://dx.doi.org/10.1029/2022JC019609, URL https://agupubs.onlinelibrary.wiley.com/doi/10.1029/2022JC019609.

Jones, K.N., Currie, K.I., McGraw, C.M., Hunter, K.A., 2013. The effect of coastal processes on phytoplankton biomass and primary production within the near-shore subtropical frontal zone. Estuar. Coast. Shelf Sci. 124, 44–55. http://dx.doi.org/10.1016/j.ecss.2013.03.003, URL https://linkinghub.elsevier.com/retrieve/pii/S0272771413001297.

Kakoulaki, G., MacDonald, D., Horner-Devine, A.R., 2014. The role of wind in the near field and midfield of a river plume. Geophys. Res. Lett. 41 (14), 5132–5138. http://dx.doi.org/10.1002/2014GL060606, URL http://doi.wiley.com/10.1002/2014GL060606.

Kalnay, E., Kanamitsu, M., Kistler, R., Collins, W., Deaven, D., Gandin, L., Iredell, M., Saha, S., White, G., Woollen, J., Zhu, Y., Leetmaa, A., Reynolds, B., Chelliah, M., Ebisuzaki, W., Higgins, W., Janowiak, J., Mo, K.C., Ropelewski, C., Wang, J., Jenne, R., Joseph, D., 1996. The NCEP/NCAR 40-year reanalysis project. Bull. Am. Meteorol. Soc. 77, 437–472. http://dx.doi.org/10.1175/1520-0477(1996)077<0437:TNYRP>2.0.CO;2, URL https://ui.adsabs.harvard.edu/abs/1996BAMS...77..437K, ADS Bibcode: 1996BAMS...77..437K.

Kidson, J.W., 2000. An analysis of New Zealand synoptic types and their use in defining weather regimes. Int. J. Climatol. 20 (3), 299–316. http://dx.doi.org/10.1002/(SICI)1097-0088(20000315)20:3<299::AID-JOC474>3.0.CO;2-B, URL https://onlinelibrary.wiley.com/doi/10.1002/(SICI)1097-0088(20000315)20:3 3C299::AID-JOC474 3E3.0.CO;2-B.

Krug, M., Swart, S., Gula, J., 2017. Submesoscale cyclones in the Agulhas current: Submesoscale Cyclones in the Agulhas. Geophys. Res. Lett. 44 (1), 346–354. http://dx.doi.org/10.1002/2016GL071006, URL http://doi.wiley.com/10.1002/2016GL071006.

Lane, E., Walters, R., Gillibrand, P., Uddstrom, M., 2009. Operational forecasting of sea level height using an unstructured grid ocean model. Ocean Model. 28 (1–3), 88–96. http://dx.doi.org/10.1016/j.ocemod.2008.11.004, URL https://linkinghub.elsevier.com/retrieve/pii/S1463500308001650.

Large, W.G., Gent, P.R., 1999. Validation of vertical mixing in an equatorial ocean model using large eddy simulations and observations. J. Phys. Oceanogr. 29 (3), 449–464. http://dx.doi.org/10.1175/1520-0485(1999)029<0449:VOVMIA>2.0.CO;2, URL http://journals.ametsoc.org/doi/10.1175/1520-0485(1999)029 3C0449:VOVMIA 3E2.0.CO;2.

Leathwick, J., Elith, J., Francis, M., Hastie, T., Taylor, P., 2006. Variation in demersal fish species richness in the oceans surrounding New Zealand: an analysis using boosted regression trees. Mar. Ecol. Prog. Ser. 321, 267–281. http://dx.doi.org/10.3354/meps321267, URL http://www.int-res.com/abstracts/meps/v321/p267-281/.

Li, J., Roughan, M., Kerry, C., Rao, S., 2022. Impact of mesoscale circulation on the structure of river plumes during large rainfall events inshore of the East Australian current. Front. Marine Sci. 9, 815348. http://dx.doi.org/10.3389/

fmars.2022.815348, URL https://www.frontiersin.org/articles/10.3389/fmars.2022.815348/full.

Liu, Y., Weisberg, R.H., Vignudelli, S., Roblou, L., Merz, C.R., 2012. Comparison of the X-TRACK altimetry estimated currents with moored ADCP and HF radar observations on the West Florida shelf. Adv. Space Res. 50 (8), 1085–1098. http://dx.doi.org/10.1016/j.asr.2011.09.012, URL https://linkinghub.elsevier.com/retrieve/pii/S0273117711006776.

Loughran, T.F., Perkins-Kirkpatrick, S.E., Alexander, L.V., 2017. Understanding the spatio-temporal influence of climate variability on Australian heatwaves: variability of Australian Heatwaves. Int. J. Climatol. 37 (10), 3963–3975. http://dx.doi.org/10.1002/joc.4971, URL https://onlinelibrary.wiley.com/doi/10.1002/joc.4971.

Malan, N., Roughan, M., Hemming, M., Ingleton, T., 2024. Quantifying coastal freshwater extremes during unprecedented rainfall using long timeseries multi-platform salinity observations. Nature Commun. 15 (1), 424. http://dx.doi.org/10.1038/s41467-023-44398-2, URL https://www.nature.com/articles/s41467-023-44398-2.

Malauene, B.S., Moloney, C.L., Lett, C., Roberts, M.J., Marsac, F., Penven, P., 2018. Impact of offshore eddies on shelf circulation and river plumes of the Sofala Bank, Mozambique channel. J. Mar. Syst. 185, 1–12. http://dx.doi.org/10.1016/j.jmarsys.2018.05.001, URL https://linkinghub.elsevier.com/retrieve/pii/S0924796317305262.

Masotti, I., Aparicio-Rizzo, P., Yevenes, M.A., Garreaud, R., Belmar, L., Farías, L., 2018. The influence of river discharge on nutrient export and Phytoplankton biomass off the central Chile coast (33 –37 S): Seasonal cycle and interannual variability. Front. Marine Sci. 5, 423. http://dx.doi.org/10.3389/fmars.2018.00423, URL https://www.frontiersin.org/article/10.3389/fmars.2018.00423/full.

Matano, R.P., Combes, V., Piola, A.R., Guerrero, R., Palma, E.D., Ted Strub, P., James, C., Fenco, H., Chao, Y., Saraceno, M., 2014. The salinity signature of the cross-shelf exchanges in the southwestern atlantic ocean: Numerical simulations. J. Geophys. Res.: Oceans 119 (11), 7949–7968. http://dx.doi.org/10.1002/2014JC010116, URL http://doi.wiley.com/10.1002/2014JC010116.

Mazzini, P.L.F., Barth, J.A., Shearman, R.K., Erofeev, A., 2014. Buoyancy-Driven coastal currents off oregon during fall and Winter. J. Phys. Oceanogr. 44 (11), 2854–2876. http://dx.doi.org/10.1175/JPO-D-14-0012.1, URL http://journals.ametsoc.org/doi/10.1175/JPO-D-14-0012.1.

Mitchell, J., Mackay, K., Neil, H., Mackay, E., Pallentin, A., Notman, P., 2012. Undersea New Zealand.

Moffat, C., Lentz, S., 2012. On the response of a buoyant plume to downwelling-favorable wind stress. J. Phys. Oceanogr. 42 (7), 1083–1098. http://dx.doi.org/10.1175/JPO-D-11-015.1, URL http://journals.ametsoc.org/doi/10.1175/JPO-D-11-015.1.

Montaño, M.M., Suanda, S.H., Souza, J.M.A.C.D., 2023. Modelled coastal circulation and Lagrangian statistics from a large coastal embayment: The case of Bay of Plenty, Aotearoa New Zealand. Estuar. Coast. Shelf Sci. 281, 108212. http://dx.doi.org/10.1016/j.ecss.2023.108212, URL https://linkinghub.elsevier.com/retrieve/pii/S0272771423000021.

Murdoch, R., Proctor, R., Jillett, J., Zeldis, J., 1990. Evidence for an eddy over the continental shelf in the downstream lee of Otago Peninsula, New Zealand. Estuar. Coast. Shelf Sci. 30 (5), 489–507. http://dx.doi.org/10.1016/0272-7714(90)90069-4, URL https://linkinghub.elsevier.com/retrieve/pii/0272771490900694.

Murphy, R.J., Pinkerton, M.H., Richardson, K.M., Bradford-Grieve, J.M., Boyd, P.W., 2001. Phytoplankton distributions around New Zealand derived from SeaWiFS remotely-sensed ocean colour data. New Zealand J. Marine Freshwater Res. 35 (2), 343–362. http://dx.doi.org/10.1080/00288330.2001.9517005, URL http://www.tandfonline.com/doi/abs/10.1080/00288330.2001.9517005.

Murray, D.L., 1975. Regional hydrology of the clutha river.

Otero, P., Ruiz-Villarreal, M., Peliz, A., 2008. Variability of river plumes off Northwest Iberia in response to wind events. J. Mar. Syst. 72 (1–4), 238–255. http://dx.doi.org/10.1016/j.jmarsys.2007.05.016, URL https://linkinghub.elsevier.com/retrieve/pii/S0924796307002503.

Powell, B.S., Leben, R.R., 2004. An optimal filter for geostrophic mesoscale currents from along-track satellite altimetry. J. Atmos. Ocean. Technol. 21 (10), 1633–1642. http://dx.doi.org/10.1175/1520-0426(2004)021<1633:AOFFGM>2.0.CO;2, URL http://journals.ametsoc.org/doi/10.1175/1520-0426(2004)021 3C1633:AOFFGM 3E2.0.CO;2.

Pyper, B.J., Peterman, R.M., 1998. Comparison of methods to account for autocorrelation in correlation analyses of fish data.

Saldías, G.S., Kipp Shearman, R., Barth, J.A., Tufillaro, N., 2016. Optics of the offshore Columbia river plume from glider observations and satellite imagery. J. Geophys. Res.: Oceans 121 (4), 2367–2384. http://dx.doi.org/10.1002/2015JC011431, URL https://onlinelibrary.wiley.com/doi/abs/10.1002/2015JC011431.

Saldías, G.S., Sobarzo, M., Largier, J., Moffat, C., Letelier, R., 2012. Seasonal variability of turbid river plumes off central Chile based on high-resolution MODIS imagery. Remote Sens. Environ. 123, 220–233. http://dx.doi.org/10.1016/j.rse.2012.03.010, URL https://linkinghub.elsevier.com/retrieve/pii/S0034425712001290.

Salinger, M.J., Renwick, J., Behrens, E., Mullan, A.B., Diamond, H.J., Sirguey, P., Smith, R.O., Trought, M.C.T., Alexander, L., Cullen, N.J., Fitzharris, B.B., Hepburn, C.D., Parker, A.K., Sutton, P.J., 2019. The unprecedented coupled ocean-atmosphere summer heatwave in the New Zealand region 2017/18: drivers, mechanisms and impacts. Environ. Res. Lett. 14 (4), 044023. http://dx.doi.org/10.1088/1748-9326/ab012a, URL https://iopscience.iop.org/article/10.1088/1748-9326/ab012a.

Schiller, R.V., Kourafalou, V.H., Hogan, P., Walker, N.D., 2011. The dynamics of the Mississippi River plume: Impact of topography, wind and offshore forcing on the fate of plume waters. J. Geophys. Res. 116 (C6), C06029. http://dx.doi.org/10.1029/2010JC006883, URL http://doi.wiley.com/10.1029/2010JC006883.

Sharples, J., Middelburg, J.J., Fennel, K., Jickells, T.D., 2017. What proportion of riverine nutrients reaches the open ocean?: Riverine nutrients reaching the ocean. Glob. Biogeochem. Cycles 31 (1), 39–58. http://dx.doi.org/10.1002/2016GB005483, URL http://doi.wiley.com/10.1002/2016GB005483.

Shchepetkin, A.F., 2003. A method for computing horizontal pressure-gradient force in an oceanic model with a nonaligned vertical coordinate. J. Geophys. Res. 108 (C3), 3090. http://dx.doi.org/10.1029/2001JC001047, URL http://doi.wiley.com/10.1029/2001JC001047.

Shchepetkin, A.F., McWilliams, J.C., 1998. Quasi-Monotone Advection Schemes Based on Explicit Locally Adaptive Dissipation. Mon. Weather Rev. 126 (6), 1541–1580. http://dx.doi.org/10.1175/1520-0493(1998)126<1541:QMASBO>2.0.CO;2, URL http://journals.ametsoc.org/doi/10.1175/1520-0493(1998)126 3C1541:QMASBO 3E2.0.CO;2.

Shchepetkin, A.F., McWilliams, J.C., 2005. The regional oceanic modeling system (ROMS): a split-explicit, free-surface, topography-following-coordinate oceanic model. Ocean Model. 9 (4), 347–404. http://dx.doi.org/10.1016/j.ocemod.2004.08.002, URL https://linkinghub.elsevier.com/retrieve/pii/S1463500304000484.

Snelder, T., Biggs, B.J., Weatherhead, M., 2010. New Zealand River Environment Classification user guide. Ministry for the Environment, Wellington, N.Z., OCLC: 669796658.

Stevens, C.L., O'Callaghan, J.M., Chiswell, S.M., Hadfield, M.G., 2019. Physical oceanography of New Zealand/Aotearoa shelf seas – a review. New Zealand J. Marine Freshwater Res. 1–40. http://dx.doi.org/10.1080/00288330.2019.1588746, URL https://www.tandfonline.com/doi/full/10.1080/00288330.2019.1588746.

Taylor, J.R., Thompson, A.F., 2023. Submesoscale dynamics in the upper ocean. Annu. Rev. Fluid Mech. 55 (1), 103–127. http://dx.doi.org/10.1146/annurev-fluid-031422-095147, URL https://www.annualreviews.org/doi/10.1146/annurev-fluid-031422-095147.

Testa, G., Masotti, I., Farías, L., 2018. Temporal variability in net primary production in an upwelling area off central Chile (36 S). Front. Marine Sci. 5, 179. http://dx.doi.org/10.3389/fmars.2018.00179, URL https://www.frontiersin.org/article/10.3389/fmars.2018.00179/full.

Walker, N.D., Wiseman, W.J., Rouse, L.J., Babin, A., 2005. Effects of river discharge, wind stress, and slope eddies on circulation and the satellite-observed structure of the mississippi river plume. J. Coast. Res. 216, 1228–1244. http://dx.doi.org/10.2112/04-0347.1, URL http://www.bioone.org/doi/abs/10.2112/04-0347.1.

Walters, R.A., Goring, D.G., Bell, R.G., 2001. Ocean tides around New Zealand. New Zealand J. Marine Freshwater Res. 35 (3), 567–579. http://dx.doi.org/10.1080/00288330.2001.9517023, URL http://www.tandfonline.com/doi/abs/10.1080/00288330.2001.9517023.

Warrick, J.A., Stevens, A.W., 2011. A buoyant plume adjacent to a headland—Observations of the Elwha River plume. Cont. Shelf Res. 31 (2), 85–97. http://dx.doi.org/10.1016/j.csr.2010.11.007, URL https://linkinghub.elsevier.com/retrieve/pii/S0278434310003584.

Waugh, S., Filippi, D., Fukuda, A., Suzuki, M., Higuchi, H., Setiawan, A., Davis, L., 2005. Foraging of royal albatrosses, Diomedea epomophora, from the Otago Peninsula and its relationships to fisheries 62. p. 12.

Willmott, C.J., 1981. On the validation of models. Phys. Geogr. 2 (2), 184–194. http://dx.doi.org/10.1080/02723646.1981.10642213, URL https://www.tandfonline.com/doi/full/10.1080/02723646.1981.10642213.

Yankovsky, A.E., Chapman, D.C., 1997. A simple theory for the fate of Buoyant coastal discharges*. J. Phys. Oceanogr. 27 (7), 1386–1401. http://dx.doi.org/10.1175/1520-0485(1997)027<1386:ASTFTF>2.0.CO;2, URL http://journals.ametsoc.org/doi/10.1175/1520-0485(1997)027 3C1386:ASTFTF 3E2.0.CO;2.